Performance Evaluation and Improvement of the Versatile Soil Moisture Budget (VSMB) Model

Prepared for Alberta Agriculture and Rural Development

Masaki Hayashi, Getachew A. Mohammed, Kim Harrer, and Christopher R. Farrow
Dept. of Geoscience
University of Calgary
2500 University Dr. NW
Calgary, Alberta, T2N 1N4
Phone: 403(220)2794 E-mail: hayashi@ucalgary.ca

Submitted: February 24, 2012

1 Introduction

Alberta Agriculture and Rural Development (AARD) needs to enhance its capacity to simulate (model) and report drought and excessive moisture conditions across the Province and provide decision makers, with measures to improve current drought and excessive moisture risk management policies, regulations and strategies as well as develop new programs. To this end, AARD is working on a new generation of year round (both growing and winter seasons) soil moisture and drought monitoring models that will make best use of data from current provincial weather station networks. The Versatile Soil Moisture Budget (VSMB) model forms the basis for the AARD's drought and excessive moisture risk assessment tool and AARD recognize the need for improvements in VSMB components, their calibration and validation, using field and laboratory measurements. To this end AARD entered into research collaboration with the Physical Hydrology Research Group of the University of Calgary. The research consists of three inter-related objectives.

Objective 1: Evaluate the performance of the VSMB model for growing season processes for barley crops by a) monitoring and analyzing the surface energy balance and soil moisture data in a barley field (see Fig. 1 for location) during July-October 2011, and b) analyzing the energy balance and soil moisture data collected in the same barley field during the growing seasons of 2009. The data are used to validate the crop coefficients and drying curves used in the existing VSMB and, if necessary, to adjust the values of these functions.

Objective 2: Develop new algorithms to represent winter processes involving snow and frozen soil, and incorporate them in the VSMB. The model will be tested using the field data collected during 2006-2009 at the University of Calgary Spy Hill hydrological research site (Fig. 1). The modified version of VSMB will be made available to AARD for its use in soil moisture modelling.

Objective 3: Collect soil samples representing typical agricultural fields from six locations in southern Alberta (Fig. 1) and analyze them for soil water retention characteristics and saturated hydraulic conductivity. The results will be used to determine the VSMB model parameters, namely field capacity, wilting point, and soil diffusivity for different soil types.

This report summarizes the research findings and presents the results in three individual chapters corresponding to the three objectives.

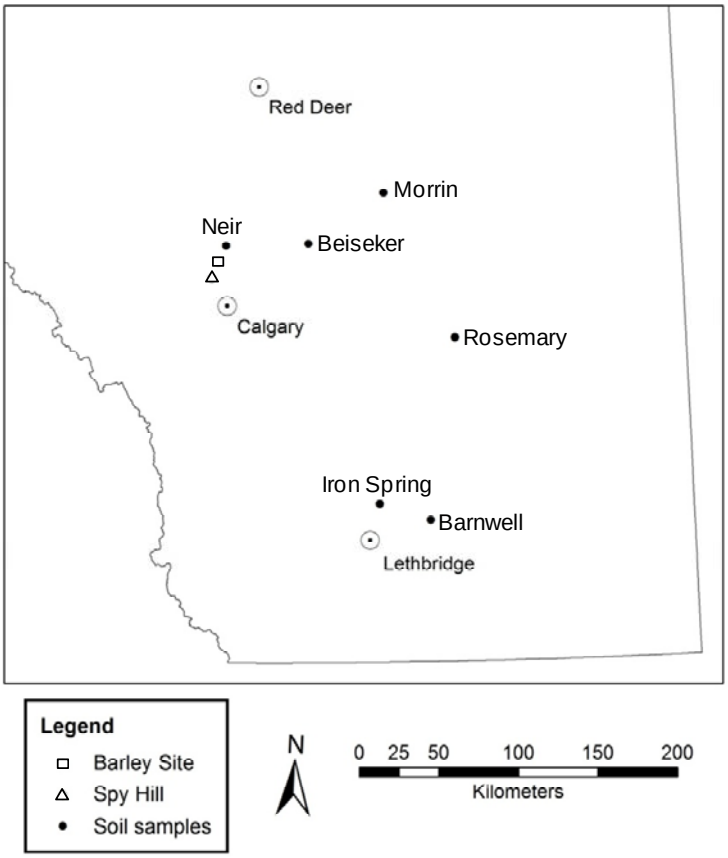

Fig. 1 Map of southern Alberta showing the location of Spy Hill Farm, Barley Site, and six soil sampling sites.

2 Evaluation of VSMB for barley growing season processes

2.1 Background information

The VSMB (Baier and Robertson, 1966) is a one-dimensional water balance model that divides the soil column into layers (typically 0.3 m in thickness) sharing common soil and plant root properties, and calculates soil water balance on a daily time step. Rainfall and snowmelt, after subtracting any surface runoff, is added to the top layer, which is subsequently distributed to lower layers by gravity drainage and gradient-driven moisture diffusion (Fig. 2). Evapotranspiration is extracted from individual layers according to the meteorological forcing, soil moisture condition, and plant growth stage (Fig. 2). The current version used by AARD is based on the modified VSMB of Akinremi et al. (1996). The numerical model and coefficients evaluated in this study were obtained from AARD in April 2007. The original code was written in SAS syntax, which was first converted to Visual Basic (Chen, 2008) and subsequently to Fortran. The conversion to Fortran was made to facilitate the future use of the VSMB to be coupled with groundwater flow models, which are commonly coded in Fortran.

2.2 Study site and field methods

This part of study was conducted using field data collected from a barley field (hereafter Barley Site) located 10 km north of the Calgary city limit (Fig. 1). The dominant soil of the Barley Site is Orthic Black Chernozem of the Antler Series and is classified as clay loam (AARD, 2012). Using the 1971-2000 normal climate data from Calgary International Airport, located 19 km south-east of the site, mean annually precipitation is 413 mm, of which 313 mm occurs during May-September (Environment Canada, 2011). Mean air temperature during May-September is 13.2 °C. The field was cropped to barley in 2007, canola in 2008, and barley in 2009, 2010, and 2011.

A meteorological station was installed in August 2004 and soil monitoring instruments were installed in July 2005. An eddy-covariance energy balance system was deployed during April-October 2009 and June-October 2011. The data used in this study were collected using a cumulative weighing precipitation gauge with an Alter windshield (Geonor, T200), an air temperature and relative humidity sensor (Campbell Scientific, HMP45C) at a height of 2.0 m above the ground surface, a four-component radiometer (Kip & Zonnen, CNR1) at 2.1 m height, and the eddy-covariance system consisting of a sonic anemometer (Campbell Scientific, CSAT3) and a krypton hygrometer (Campbell Scientific, KH20) at 2.3 m height (Fig. 3). The eddy-covariance data were processed through the instrumental and tilt correction, and energy balance correction as described in Hayashi et al. (2010).

Soil water content was monitored using capacitance probes (Campbell Scientific, CS616) at 0.1, 0.3, and 0.6 m depths, which were individually calibrated in situ using the collocated time domain reflectometry (TDR) probes. In addition to the automated capacitance probes, soil water content was manually monitored weekly at 1.0 m depth using the TDR method. Thermocouples were installed at depths of 0.0, 0.2, 0.4, 0.6, 0.8, 1.0 and 1.5 m to measure soil temperature. Ground heat flux was measured using a heat flux transducer (Campbell Scientific, HFT3) at a depth of 5 cm, which was calibrated in situ using the thermo-calorimetric method (Mayocchi and Bristow, 1995). All data were averaged and recorded at 30-minute interval (except for precipitation at hourly interval) using dataloggers (Campbell Scientific, CR10X and CR3000).

In 2009 and 2011 study periods, crop height was measured on a weekly schedule both in the instrumented soil pit and the barley field outside of the soil pit using a metal ruler at five locations, and the average value was recorded. In the 2011 study period, crop growth stage was monitored using the Zadoks growth stage chart (Anderson et al., 1985).

2.3 VSMB model parameters

Soil samples were collected in 100 cm^3 sample rings from depths of 0.1, 0.3, 0.6, and 1.0 m in July 2005. Porosity of samples (θ_{sat}) was determined gravimetrically by measuring the saturated and oven-dry weights of the samples, and water retention characteristics was determined with the pressure plate extractor method (Dane and Hopmans, 2002). The field capacity of the soil at 0.1, 0.3, and 0.6 m depth was determined by the analysis of 30-min time series of water content data after large rainfall events as described by Hayashi et al. (2010), and the wilting point of the soil at these depths were taken to be the lowest recorded values during dry periods. The volumetric water content (θ) at field capacity (θ_{FC}) and wilting point (θ_{WP}) of deeper soil horizon were assumed to be the same as those at 0.6 m depth based on the similar water retention characteristics between 0.6 m and 1.0 m soil samples. The porosity, field capacity, and wilting point of the VSMB soil layers are calculated from the point values at 0.1, 0.3, 0.6, and 1.0 m and listed in Table 1.

The VSMB estimates evapotranspiration from individual soil layers as a product of potential evaporation (E_p, mm) and the empirical factors dependent on soil moisture and plant conditions. Total evapotranspiration (E, mm) from all layers is

$$E = \sum_{i=1}^{n} \left[E_p \times R_i \times f_{DC}(S_i / S_{Ci}) \right] \quad (1)$$

where R_i and f_{DC} are defined below, $S_i = \theta_i - \theta_{WPi}$, and $S_{Ci} = \theta_{FCi} - \theta_{WPi}$. Potential evaporation is calculated using the method of Priestley and Taylor (1972), whereby net radiation is estimated from the site latitude and the day of the year (Akinremi et al., 1996).

The R_i in Eq. 1 is a plant-specific root extraction coefficient, which is dependent on the crop's growth stage. It was a simple constant in the original VSMB, and Baier et al. (1979) modified it (see Eq. 2 below) to account for the effects of plant roots seeking deeper moisture sources when the moisture in shallower layers becomes depleted. The R_i is computed sequentially as

$$R_1 = r_1$$

$$R_i = r_i + r_i \sum_{j=1}^{i-1} R_j (1 - S_j / S_{Cj}) \quad \text{for } i \geq 2 \quad (2)$$

where r_i are dimensionless constants that are specific to soil depth and plant growth stage. The r_i values used in the present study are default values for spring wheat used by AARD (Table 2).

The f_{DC} in Eq. 1 is an empirical "drying curve" function, which is equal to 0 at wilting point ($S_i/S_{Ci} = 0$) and monotonically increases with S_i/S_{Ci} towards 1. The f_{DC} is given by

$$f_{DC}(x) = C_n (x / C_r)^{C_m C_n C_h} + x(C_m / C_r)(1 - x / C_r)^{C_n} \quad (3)$$

where C_m, C_n, C_h, and C_r are dimensionless fitting parameters. The values of coefficient in the present study are default values for spring wheat used by AARD (Table 3).

The VSMB simulates crop growth using the bio-meteorological approach of Robertson (1968). The VSMB determines the seeding date for spring wheat based on daily mean air temperature, precipitation, and soil moisture condition; and the harvest date based on daily minimum air temperature. When the meteorological conditions for seeding have not been met by

June 30, then the VSMB sets the seeding date to June 30. Similarly, the harvest date is set to September 30 if minimum air temperature condition has not been satisfied by this date. Preliminary examination of the field data showed that the seeding and harvest dates predicted by the VSMB would be unrealistically late compared to the actual seeding and harvest dates. Therefore, the VSMB was modified so that the latest dates of seeding and harvest are June 10 and September 10, respectively, to reflect the condition of the study site. No other modification was made to the crop growth algorithms of the VSMB.

The initial soil moisture for the model simulation is specified using the observed soil moisture data on May 1 of each year. The soil water content in the 0-0.3 m layer is given by the weighted average of observed values at 0.1 m and 0.3 m, the 0.3-0.6 m layer by the simple mean of observed values at 0.3 m and 0.6 m, the 0.6-0.9 m by the weighted average of observed values at 0.6 m and 1.0 m, and 0.9-1.2 m by the observed value at 1.0 m. The same scheme was used for the comparison of observed and simulated water content in the four soil layers.

2.4 Model evaluation using the 2009 data

The 2009 study period (May 1 - September 30) was relatively dry compared to normal years. Total precipitation recorded at the Calgary International Airport (YYC) was 192 mm, whereas the 1971-2000 normal is 313 mm. Total precipitation at the study site was 201 mm (Table 4), of which the majority (142 mm) occurred during a 50-day period between June 30 and August 18 (Fig. 4a). The VSMB simulated the seasonal pattern of evapotranspiration reasonably well (Fig. 4b), except during June 11-July 3, while the simulated crop stage was 2 (Fig. 4f). During this period, the crop had already germinated and grown to a height of 0.25 to 0.3 m (Fig. 4e). The crop coefficients (r_i) in the VSMB (Table 1) may be under-representing the activity of barley during Stage 2.

Daily evapotranspiration data were only available for 82 out of 152 days due to frequent data gaps resulting from the malfunctioning of humidity sensor during precipitation events. This problem is common to all eddy-covariance measurements using open-path humidity sensors like the krypton hygrometer used in our system. Total evapotranspiration during the study period was estimated by taking an average of observed values during three separate periods (May 1-June 15, June 16-September 10, and September 10-30), multiplying the average value by the number of days in each period, and adding them up. Estimated total evapotranspiration was 317 mm (Table 4). The simulated total evapotranspiration was 319 mm (Table 4), which is reasonably close to the observed value. The cross plot of observed and simulated evapotranspiration for those days with available data (Fig. 5a) indicates a relatively large scatter of data and a slight negative bias of simulated data. The model performance with respect to evapotranspiration is quantified using the root-mean-squared error (RMSE) and mean bias error (MBE) given by

$$\text{RMSE} = \sqrt{\frac{1}{n}\sum_{i=1}^{n}(x_{sim} - x_{obs})^2} \tag{4}$$

$$\text{MBE} = \frac{1}{n}\sum_{i=1}^{n}(x_{sim} - x_{obs}) \tag{5}$$

where x_{sim} and x_{obs} are simulated and observed values, respectively, of a variable and n is the number of data points. The RMSE and MBE for the 2009 data set were 0.64 mm d^{-1} and -0.08 mm d^{-1}, respectively.

The crop height in instrumented soil plot was lower than the surrounding barley field (Fig. 4e), presumably because we did not apply fertilizer to the soil plot this year. The crops in the field were harvested on September 9.

The initial soil moisture condition on May 1 was relatively dry. The VSMB simulated the soil moisture in these two zones reasonably well (Figs. 4c and 4d). The observed change in soil moisture storage (ΔS, mm) during the study period was -105 mm (Table 4), whereas the simulated ΔS was -120 mm (Table 4).

The water balance of the entire soil profile is

$$P - E - R_{off} - G - \Delta S = 0 \quad (6)$$

where P (mm) is precipitation, R_{off} (mm) is surface runoff, and G (mm) is the amount of drainage from the bottom of soil profile (Fig. 2). The right hand side of Eq. (6) is not usually zero for the field data, reflecting the uncertainty and errors in measuring and estimating individual terms on the left hand side. The non-zero value of the right hand side is called the water balance residual (W_{res}, mm). The magnitude of errors associated with soil moisture measurement is expected to be in the order of 10-20 mm, and the error in evapotranspiration measurement is expected to be in the order of 5-10 %. Therefore, W_{res} in the order of 20-30 mm can be accounted for by the measurement errors, while a greater magnitude of W_{res} may indicate missing processes.

The W_{res} in Table 4 is calculated assuming that G is negligible. The small magnitude of W_{res} suggests that G is indeed negligible and E and ΔS are reasonably well estimated. Total E and ΔS based on the VSMB simulation are consistent with the observed values (Table 4), indicating a good performance of the model for this study period.

2.5 Model evaluation using the 2011 data

The 2011 study period was much wetter than normal years. Total precipitation recorded at YYC during May-September was 368 mm, compared to the 1971-2000 normal of 313 mm. The pre-seeding period of April and May was particularly wet with total precipitation at YYC of 144 mm, compared to the normal of 84 mm. A series of heavy rain events (total of 93 mm) during May 19-28 (Fig. 6a) resulted in a very moist soil condition when the field monitoring with the complete set of instrument started on June 3 (Fig. 6c). Total precipitation at the study site during the monitoring period (June 3-Septebmer 30) was 206 mm (Table 4).

The VSMB simulated the seasonal pattern of evapotranspiration reasonably well (Fig. 6b). Total observed evapotranspiration during the monitoring period was estimated to be 330 mm, whereas the simulated evapotranspiration was 310 mm (Table 4). The cross plot of observed and simulated evapotranspiration for those days with available data (Fig. 5c) indicates a relatively large scatter of data and a slight negative bias of simulated data. The RMSE and MBE of the simulated evapotranspiration were 0.57 mm d^{-1} and -0.11 mm d^{-1}, respectively.

The barley crops rapidly grew both in the field and the instrumented soil plot, and reached the maximum height on August 9 (Fig. 6e) and the Zadoks Stage 75 (kernel with medium milk) on August 24 (Fig. 6f). The crops were harvested several days after September 6, most likely on September 9 or 10.

The VSMB substantially overestimated the soil moisture in the 0-0.6 m zone (Fig. 6c), and slightly overestimated it in the 0.6-1.2 m zone (Fig. 6d). The observed change in soil moisture storage (ΔS, mm) during the monitoring period was -187 mm (Table 4), whereas the simulated ΔS was -124 mm (Table 4). No surface runoff was observed in the field, but the VSMB simulated a small, but a noticeable amount of runoff (1.2 mm) during the period (Table 4), most

of which occurred during a rain event on June 16-18. The large magnitude of water balance residual of the field data suggest that the assumption of negligible G was most likely violated. A sizable amount of soil water likely percolated below the deepest (1.0 m) soil moisture sensor. The VSMB simulated 19 mm of G (Table 4), but this was not sufficient to account for a large difference between observed and simulated ΔS (Table 4).

2.6 Preliminary adjustment of model coefficients

Substantial overestimation of soil moisture in the 2011 study period (Figs. 6c,d) suggest that the model performance may be improved by adjusting crop coefficients and drying curve parameters, thereby changing the timing and amount of evapotranspiration. To assess the feasibility of this approach, the root extraction coefficient for the top soil layer was increased to 0.70 in Stage 2 and 0.80 in Stage 3. This was an attempt to capture the relatively high evapotranspiration rates during June and early July (Figs. 4b and 6b). Also, the drying curve parameters for grass pasture (Table 3) were used in an attempt to increase evapotranspiration rates during a relatively dry period of July and August.

The VSMB simulation for the 2011 study period using the adjusted model parameters show a somewhat improved match between the observed and simulated evapotranspiration (Fig. 7d) and soil moisture (Figs. 7e,f). The comparison of total E and ΔS between the observed and simulated values clearly suggests an improvement (Table 4), however, the magnitude of simulated ΔS is still too small. The cross plot of observed and simulated evapotranspiration for 2011 indicates the model with the adjusted parameters (Fig. 5d) gives slightly better results than the model with default parameters (Fig. 5c).

For the 2009 study period, adjusting the model parameters did not noticeably improve the simulation results (Figs. 7a-c). The cross plot of evapotranspiration data (Figs. 5a,b) indicate a slight improvement with the adjusted parameters, but the comparison of total E and ΔS indicate slightly larger differences between observed and simulated E and ΔS for the adjusted model.

2.7 Concluding remarks on the VSMB testing for barley crops

The VSMB with default parameters for crop coefficients and dry curve function performed reasonably well for the relatively dry summer of 2009. It should be noted, however, the parameters for water retention were determined using the field data, and the seeding and harvest dates were adjusted to reflect the condition of the region. Without these adjustments, the model performance may have been much poorer. The performance of the same model in the wet summer of 2011 was somewhat poorer than in 2009, particularly in terms of soil moisture storage. By the end of the study period (September 30), the model overestimated soil moisture in the 0-0.6 m zone by 24 mm (Fig. 6c), and 0.6-1.2 m zone by 8 mm (Fig. 6d). This magnitude of error may or may not be acceptable depending on the application of the model.

The model performance can be improved slightly by adjusting the crop coefficients and drying curve function, but such adjustment may require further field testing at multiple locations. Until such opportunity becomes available, it is sensible to use the model with default crop coefficients and drying curve function but adjust seeding and harvest date, as well as soil water retention parameters.

Table 1 Soil water storage parameters used in the VSMB: volumetric water content at saturation (θ_{sat}), field capacity (θ_{FC}), and wilting point (θ_{WP}).

Depth (m)	θ_{sat}	θ_{FC}	θ_{WP}
0-0.3	0.65	0.32	0.14
0.3-0.6	0.50	0.35	0.14
0.6-0.9	0.50	0.35	0.14
0.9-1.2	0.50	0.35	0.14

Table 2 Root extraction coefficients (r_i) for spring wheat.

Depth (m)	Stage 1	Stage 2	Stage 3	Stage 4	Stage 5
0-0.3	0.5	0.55	0.75	0.80	0.80
0.3-0.6	0.05	0.10	0.25	0.25	0.25
0.6-0.9	0.01	0.02	0.15	0.15	0.15
0.9-1.2	0.01	0.01	0.05	0.05	0.05

Table 3 Parameter values for the drying curve function.

	C_m	C_n	C_h	C_r
Wheat default	0.27	0.90	0.30	1.58
Grass default	0.5	0.9	0.05	1.00

Table 4 Total soil water balance components: Precipitation (P), evapotranspiration (E), soil water storage change (ΔS) in the 1.2 m soil column, runoff (R_{off}), deep percolation (G), and water balance residual (W_{res}). Note that the duration of water balance period is 153 days (May 1 - September 30) in 2009 and 120 days (June 3 - September 30) in 2011.

	Field observation (mm)					VSMB - default (mm)				VSMB - adjusted (mm)			
Year	P	E	ΔS	R_{off}	W_{res}	E	ΔS	R_{off}	G	E	ΔS	R_{off}	G
2009	201	317	-105	0	-11	319	-120	0.5	0	325	-126	0.2	0
2011	206	330	-187	0	64	310	-124	1.2	19	338	-148	0.9	15

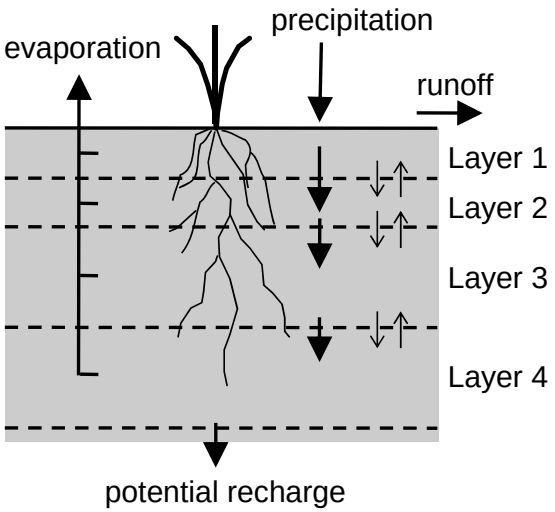

Fig. 2 Schematic diagram of the Versatile Soil Moisture Budget (VSMB) model.

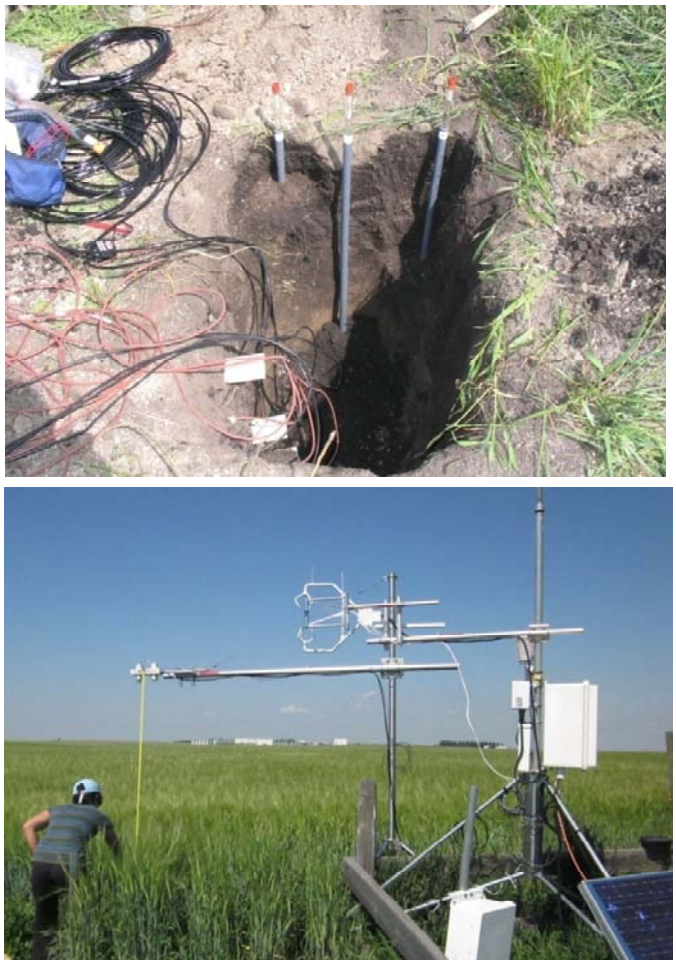

Fig. 3 Photographs of the instrumentation at the Barley Site. Top: soil pit with tensiometers and soil moisture sensors (July 2005). Bottom: eddy-covariance energy balance system (June 2011).

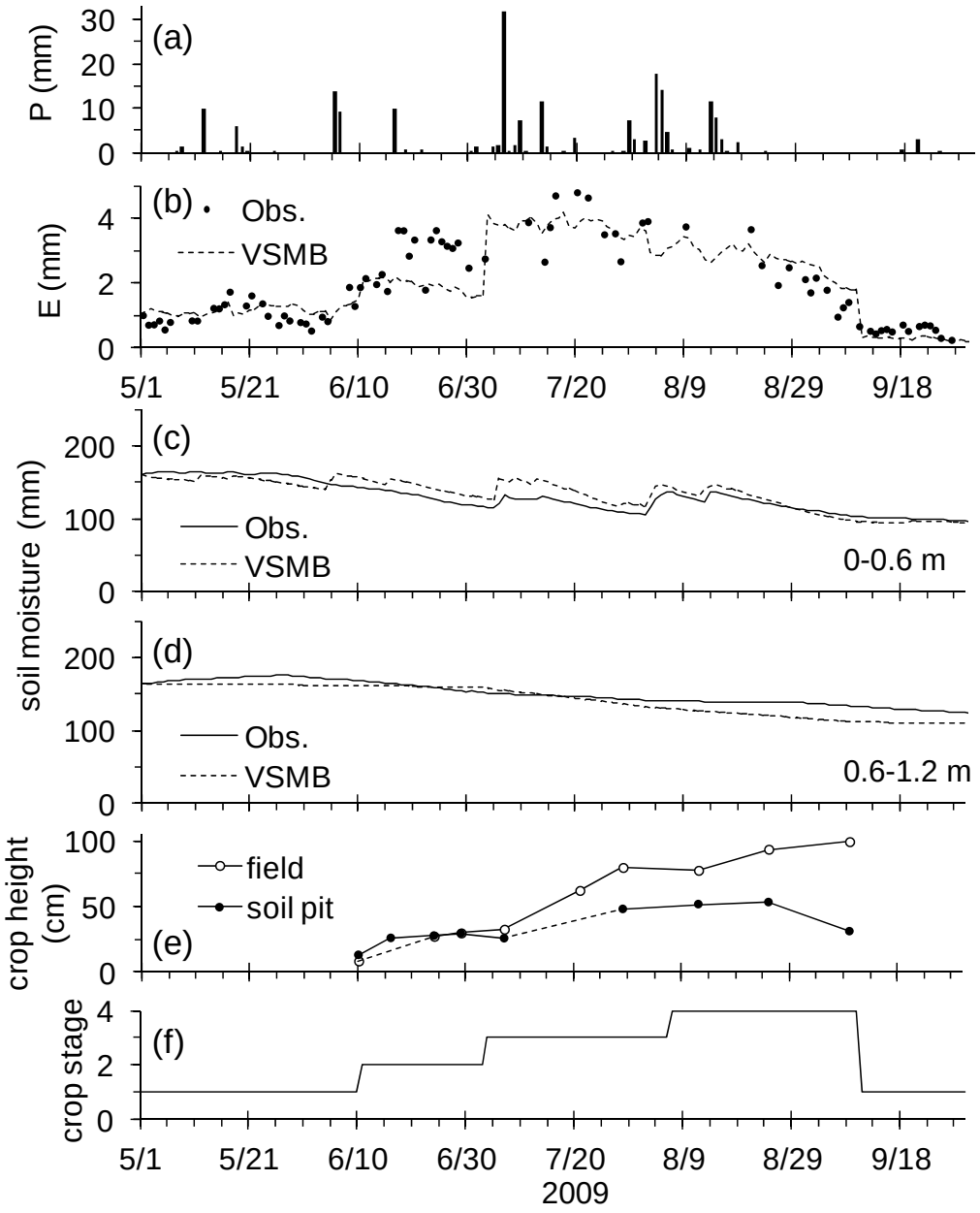

Fig. 4 The results for 2009. (a) Daily precipitation (*P*). (b) Observed and simulated daily evapotranspiration (*E*). (c) Observed and simulated total soil moisture (mm) in the top soil two layers (0-0.6 m). (d) Observed and simulated total soil moisture in the third and fourth soil layers. (e) Observed crop height in the barley field and in the instrumented plot (soil pit). (f) Simulated crop stages.

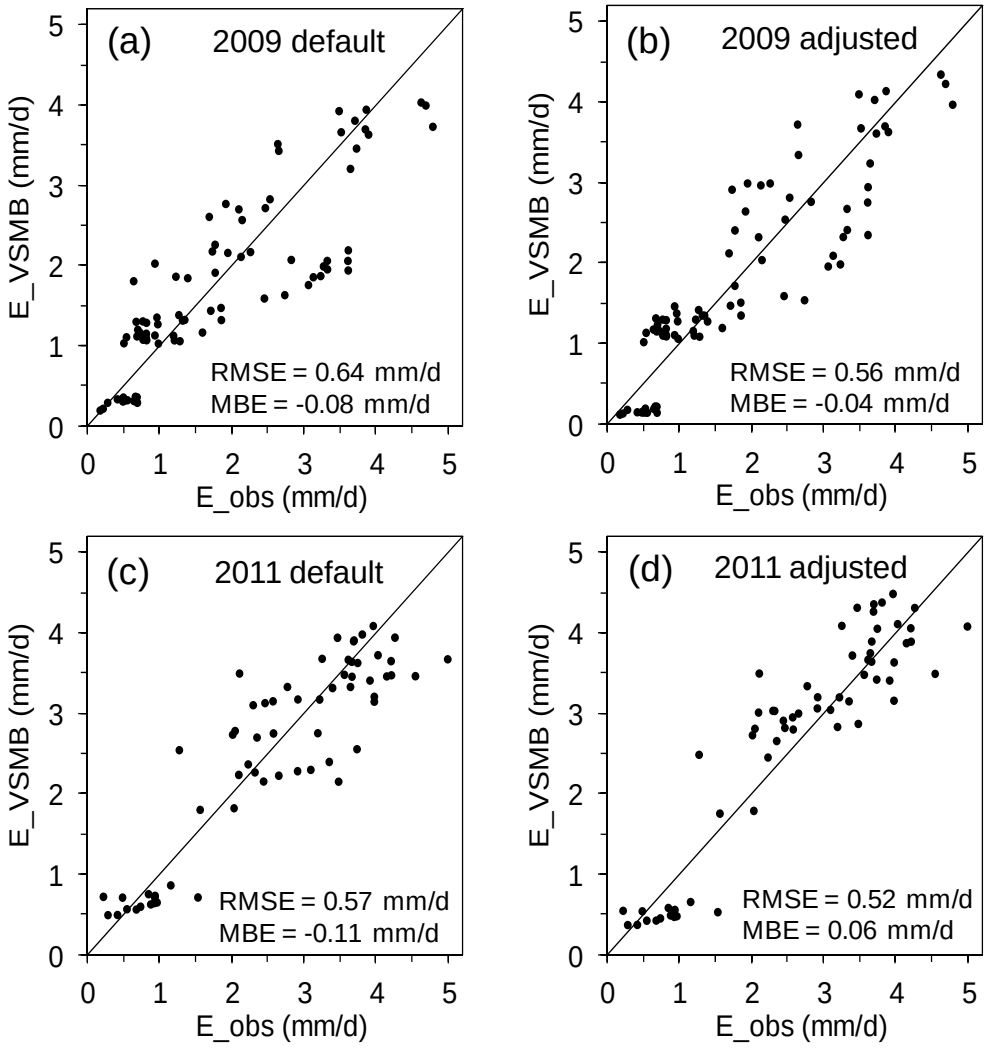

Fig. 5 Cross plot observed (E_obs) and simulated (E_VSMB) of daily evapotranspiration. Data points are shown only for the days in which the E_obs is available. VSMB simulation uses the default crop stage and drying curve parameters for (a) and (c), and the modified (see texts) parameters for (b) and (d). The solid line shows the slope of 1:1. The values indicate root-mean-squared error (RMSE) and mean bias error (MBE).

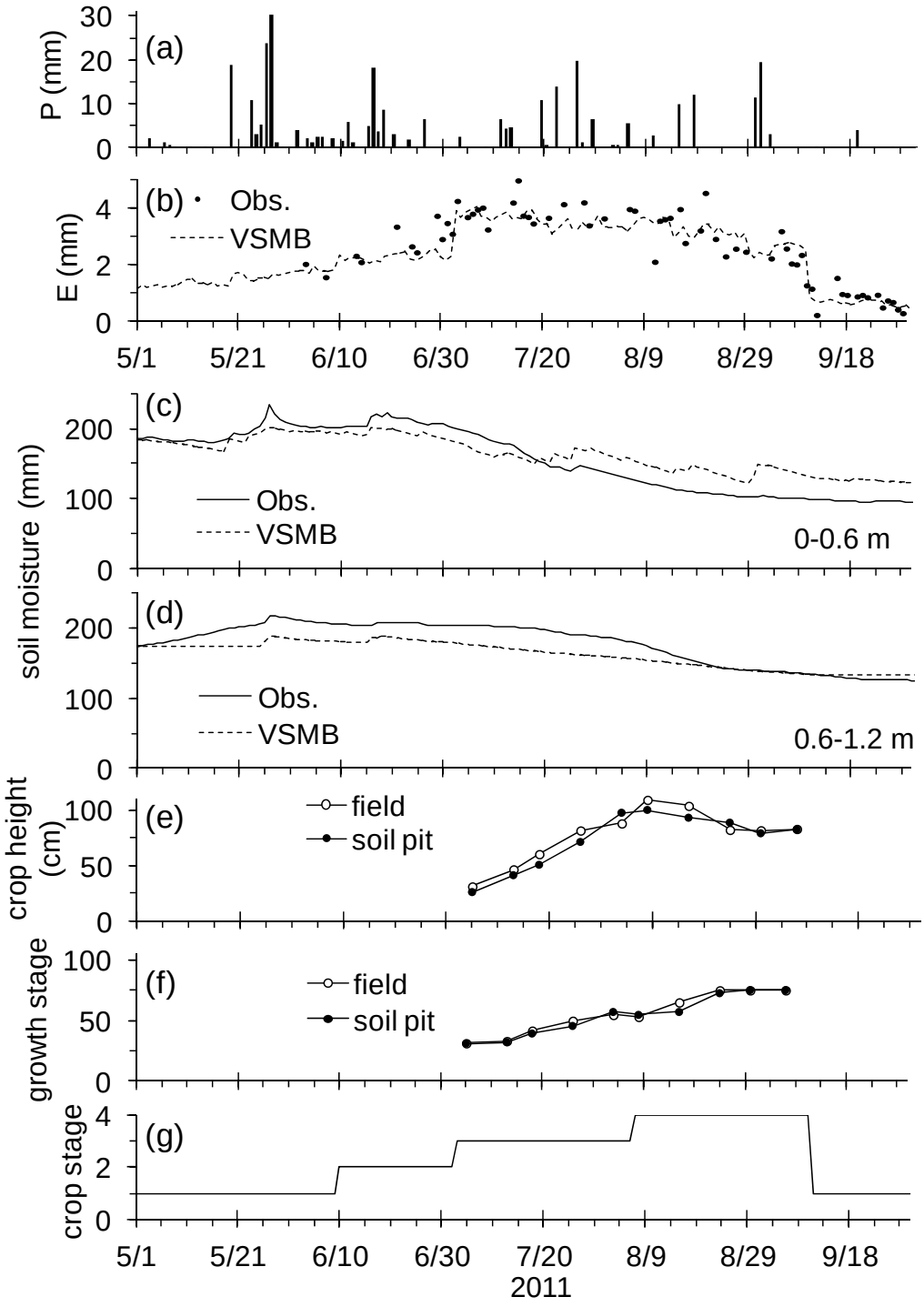

Fig. 6 The results for 2011. (a) Daily precipitation (*P*). (b) Observed and simulated daily evapotranspiration (*E*). (c) Observed and simulated total soil moisture (mm) in the top soil two layers (0-0.6 m). (d) Observed and simulated total soil moisture in the third and fourth soil layers. (e) Observed crop height in the barley field and in the instrumented plot (soil pit). (f) Observed Zadoks growth stages. (f) Simulated crop stages.

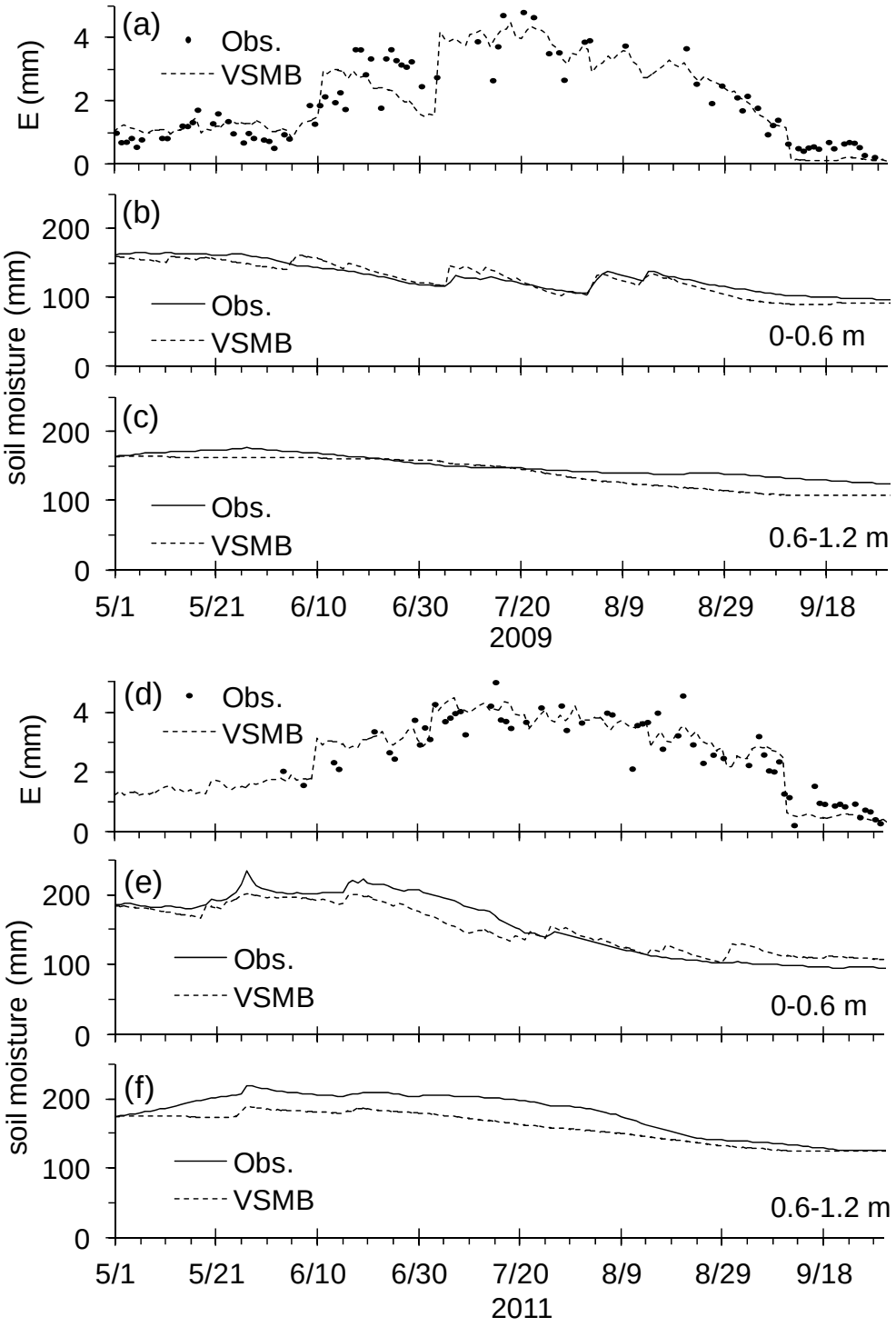

Fig. 7 Comparison of observed and simulated data for 2009 and 2011. VSMB simulations use the modified parameters for crop coefficients and drying curve. (a) Daily evapotranspiration (*E*) for 2009. (b) Total soil moisture (mm) in the top soil two layers (0-0.6 m) for 2009. (c) Total soil moisture in the third and fourth soil layers for 2009. (d) Daily evapotranspiration (*E*) for 2011. (e) Total soil moisture (mm) in the top soil two layers (0-0.6 m) for 2011. (f) Total soil moisture in the third and fourth soil layers for 2011.

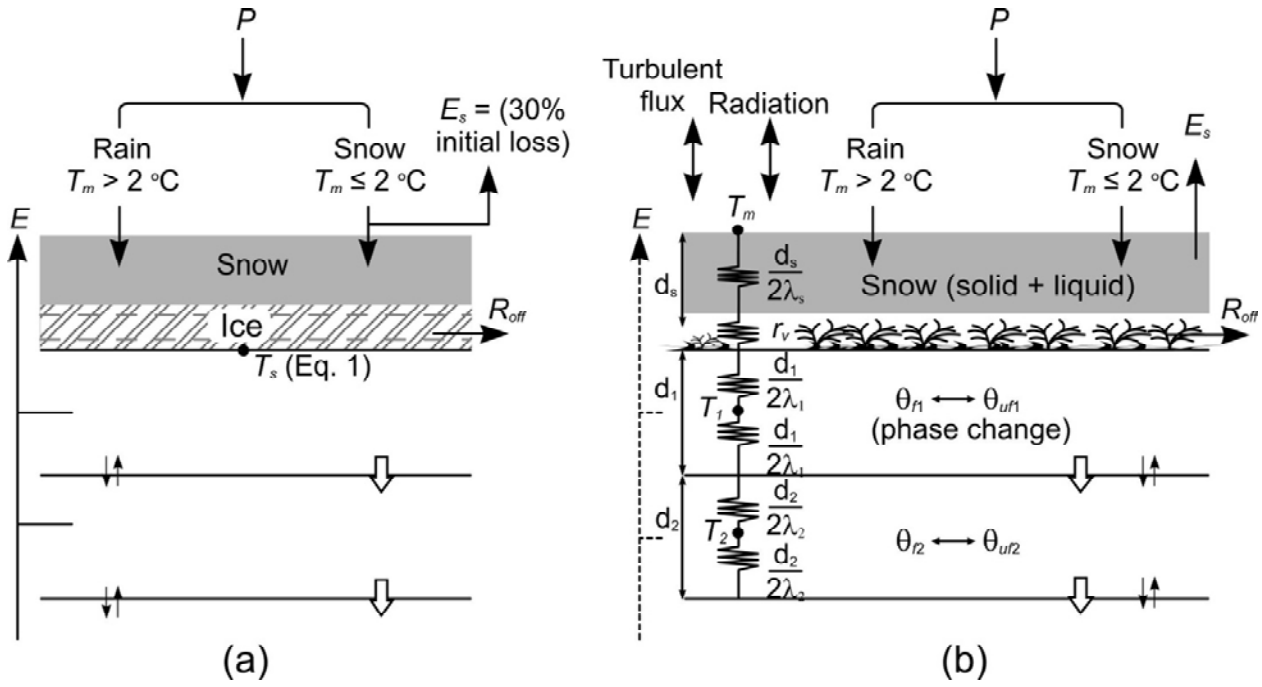

Fig. 8 Schematic diagrams of winter processes in (a) the old VSMB model and (b) the new VSMB model modified in this study. The symbols and processes are explained in the texts.

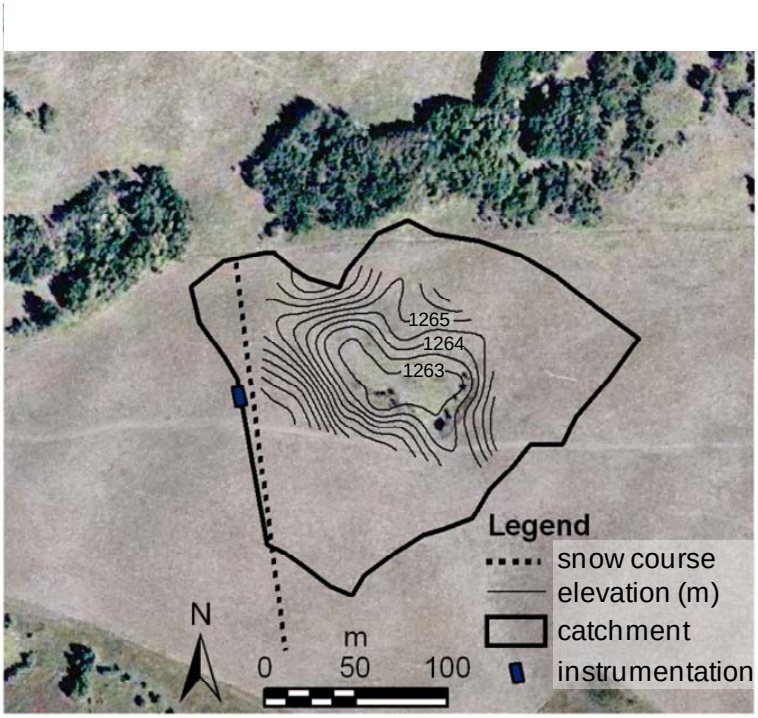

Fig. 9 Aerial photograph of the Spy Hill site showing the location of instrumented site, snow survey course, and the extent of the catchment draining to a depression. Elevation contours are derived from detailed survey data (Jackson 2008) and drawn at 0.5 m interval.

3 Improved representation of winter processes in the VSMB

3.1 Background information

A modified version of the VSMB reported by Hayashi et al. (2010) is used as the base model to implement the new winter process algorithms. This version is referred to as the "old VSMB" (VSMBo) to distinguish it from the new VSMB (VSMBn) incorporating the algorithms. In the following, the winter process algorithms in the VSMBo are briefly described.

Given daily precipitation (P) and mean air temperature, $T_m = (T_{max} + T_{min})/2$, P is regarded as rain if $T_m > 2$ °C and snow otherwise (Fig. 8a). To account for sublimation loss, a user specified fraction (typically 30 %) of snowfall is immediately removed and the rest accumulates on the ground. Snowmelt is calculated using the temperature-index method with coefficients that vary depending on the latitude and the day of year (McKay 1964). While the temperature index may represent the melt energy reasonably well, the release of melt water is influenced by complex storage and freezing-melting processes within the snowpack. The VSMBo represents the storage of melt water using a simple algorithm, which generates "potential snowmelt" from the temperature index and stores it in the snowpack as "ice", simulating the effects of melt water refreezing at night (Fig. 8a). If potential snowmelt remains positive after all snow has been transformed to ice, the model releases part or all of ice as melt water. The VSMBo uses the Priestley and Taylor (1972) method to compute potential evaporation for the days that have positive net radiation (Akinremi et al. 1996). The VSMBo uses potential evaporation to represent evaporation of melt water from the snowpack when the snow water equivalent (SWE) is greater than 10 mm. The model does not calculate sublimation when SWE is less than 10 mm, but instead extracts evapotranspiration from the soil layers using the same algorithm as the plant growing season.

Akinremi et al. (1996) adopted the temperature algorithm of the EPIC model (Williams et al. 1990) to calculate soil surface temperature (T_s, °C) by

$$T_s = I_s T_{m\text{-}1} + (1 - I_s)[T_m + (T_{max} - T_{min})/4 + T_{m\text{-}1} + T_{m\text{-}2}]/3 \quad (7)$$

where $T_{m\text{-}1}$ and $T_{m\text{-}2}$ (°C) are daily mean air temperature of one and two days, respectively, before the current day; and I_s is a dimensionless variable representing the effects of thermal insulation by the snowpack having snow water equivalent (SWE) of C (mm);

$$I_s = C / [C + \exp(2.303 - 0.2179C)]. \quad (8)$$

When $T_s \leq 0$ °C (i.e. frozen condition), daily surface runoff (R_{off}, mm) is calculated using

$$R_{off} = W_{in} \times (\theta / \theta_{FC}) \quad (9)$$

where W_{in} (mm) is the daily amount of water input, which include snowmelt and rainfall, θ is the volumetric water content of the first soil layer, and θ_{FC} is its volumetric water content at field capacity (Akinremi et al. 1996). The remaining portion of W_{in} is added to the top layer as infiltration. Soil water in excess of θ_{FC} is drained daily regardless of T_s, which maintains $\theta / \theta_{FC} \leq 1$. Note that the VSMBo does not distinguish liquid water from ice, and θ is the total water content. When $T_s > 0$ °C, the Curve Number method (NRCS 2004) is used to calculate R_{off} from W_{in} and the soil type and antecedent moisture condition (see 3.7 Appendix).

3.2 Field site and methods

The field data were collected at a grass pasture site of Spy Hill Farm in Calgary, Alberta (Fig. 1). The site has Orthic Black Chernozem soil of the Dunvargan Series having loam to clay loam

texture (AARD, 2012), which is underlain by 10-13 m thick glacial till consisting of 10-20% sand, 45-60% silt and 20-45% clay (van Dijk 2005). The topography is undulating with numerous depressions, typical of the Canadian prairies, and landcover is dominated by smooth brome (*Bromus inermis*), with some alfalfa (*Medicago sativa*), tufted hair grass (*Deschampsia caespitosa*), smooth meadow grass (*Poa pratensis*), and Canadian thistle (*Cirsium arvense*) (Zaitlin et al. 2007). Using the 1971-2000 normal climate data from Calgary International Airport, located 14 km east of Spy Hill, mean annually precipitation is 413 mm, of which 86 mm occurs during the winter months of November-April (Environment Canada, 2011). Note that the precipitation data in the National Climate Data Archive (Environment Canada, 2011) are not corrected for wind under-catch and, hence substantially underestimate solid precipitation (Craig Smith, personal communication). Monthly mean temperature is -8.9 °C in January and 16.2 °C in July.

The meteorological and soil monitoring instruments were installed in June 2006 in a relatively flat location (Fig. 9) (Hayashi et al. 2010). The instruments included temperature and relative humidity sensor (Campbell Scientific, HMP45C) at a height of 1.6 m above the ground surface, a four-component radiometer (Kip & Zonnen, CNR1) at 1.7 m height, wind sensor (R.M. Young, 05103) at 3.1 m height, snow depth sensor (Campbell Scientific, SR50) at 1.3 m height, and an eddy-covariance system consisting of a sonic anemometer (Campbell Scientific, CSAT3) and a krypton hygrometer (Campbell Scientific, KH20) at 1.9 m height (Fig. 10). The eddy-covariance data were processed through the instrumental and tilt correction as described in Hayashi et al. (2010). The energy balance correction of eddy-covariance data is discussed in results. A cumulative weighing precipitation gauge with an Alter windshield (Geonor, T200), along with a wind sensor (Met-One, 014A), was installed in a clearing inside a small patch of trees providing wind shelter, located 400 m north of the instrumented site. The precipitation data were corrected for wind under-catch of snow by applying Eq. 4 of Smith (2007) for hourly data when the air temperature was below 2°C. Soil water content was monitored using capacitance probes (Campbell Scientific, CS616) at 0.1, 0.3, 0.6, and 1.0 m depths, which were individually calibrated *in situ* under unfrozen conditions using the collocated time domain reflectometry (TDR) probes (Hayashi et al. 2010). It is assumed that the same calibration curves are applicable for estimating unfrozen water content under frozen conditions, although such an assumption may introduce some degree of error (e.g. Watanabe and Wake 2009). Thermocouples were installed at depths of 0.0, 0.2, 0.4, 0.6, 0.8, 1.0 and 1.5 m to measure soil temperature. Ground heat flux was measured using a heat flux transducer (Campbell Scientific, HFT3) at a depth of 5 cm, which was calibrated *in situ* using the thermo-calorimetric method (Mayocchi and Bristow, 1995). All data were averaged and recorded at 30-minute interval (except for precipitation at hourly interval) using dataloggers (Campbell Scientific, CR10X and 23X).

Due to the undulating topography and wind-induced snow drift, a point measurement of snow depth does not represent the actual amount of snow accumulation in the study area. Snow depth was measured using a metal ruler on a weekly to bi-weekly schedule at 1 m interval along a 200-m snow course encompassing high and low parts of the undulating terrain (Fig. 9), and snow samples were collected at 50 m interval using a 7.0 cm diameter aluminum snow tube (Fig. 10). The samples were transferred to a sealable bag and weighed in the laboratory to determine snow density. The average snow water equivalent was calculated from the average snow depth and density.

It is very difficult to monitor average snowmelt runoff over a scale comparable to that of snow course and eddy-covariance measurement. In this study, snowmelt runoff is estimated by

monitoring the depth of runoff water collected in a depression located east of the instrumented site (Fig. 9) using a pressure transducer (In-Situ, Mini-Troll). The depth of water was converted to volume using a depth-area-volume relationship (Hayashi and van der Kamp, 2000) with coefficients determined using the high-resolution elevation survey data (Jackson, 2008). The amount of daily runoff was estimated from the volume change, direct precipitation input, and infiltration loss estimated from the rate of steady night-time water level recession when no snowmelt was occurring. The volume of daily runoff was divided by the catchment area (30,000 m^2) of depression (Fig. 9) to estimate average runoff (mm). This method neglects the loss of water to the unsaturated soil during the initial flooding period, and hence underestimates snowmelt runoff (van der Kamp et al., 2003), particularly when the total amount of runoff is relatively small compared to the initial loss.

The hydraulic properties of soil samples collected from the instrumented site were determined and reported by Hayashi et al. (2010). To determine soil thermal properties and freezing characteristics, a soil sample was collected in September 2008 from a depth of 20 cm, oven dried, and ground to powder. The dry powder was mixed with water to prescribed water contents, and repacked in an acrylic tube (64 mm diameter, 70 mm height) to a dry bulk density of 1,440 kg m^{-3} (Toshihiko Momose, personal communication). Thermal conductivity was measured using the twin heat probe method (Hiraiwa and Kasubuchi, 2000). Similarly, the dry powder sample was mixed with water to a volumetric water content of 0.35 and repacked in an aluminum tube (94 mm diameter, 105 mm height) to a dry bulk density of 1,440 kg m^{-3}. A TDR probe and thermistors were inserted to the sample tube, which was placed in a controlled temperature bath filled with antifreeze fluid. The temperature of the bath was gradually lowered from 1 °C to -17 °C and back to 1 °C over a period of 24 hours, and sample temperature and apparent dielectric permittivity were monitored using a TDR system and datalogger (Campbell Scientific, TDR100 and CR1000). The TDR wave form was analyzed with WATTDR software (Redman, 2000), and a soil-specific calibration curve was used to calculate unfrozen water content from apparent dielectric permittivity assuming that the same calibration curve is applicable to frozen and unfrozen conditions.

3.3 Model modification

3.3.1 Snow accumulation and melt

Preliminary evaluation of the VSMBo showed that the temperature index algorithm has difficulty in representing the effects of mid-winter foehn (i.e. Chinook) events, suggesting that the model performance will be improved by incorporating an energy-balance algorithm. Among several commonly used models, the Utah Energy Balance (UEB) model (Tarboton et al., 1995) was chosen for its computational efficiency. The UEB computes the amount of snowmelt from the energy balance of a lumped system of snowpack and underlying top soil, forced by air temperature, relative humidity, wind speed, incident short-wave radiation, and precipitation. The meltwater is partially retained in and released from the snowpack depending on its hydraulic properties.

In the VSMBn, the UEB model computes SWE and snowmelt on sub-daily time steps from the meteorological data and soil temperature calculated by the soil freezing-thawing algorithm (Fig. 8b), and it returns daily average snowpack thickness and total meltwater input to the soil freezing-thawing algorithm. Sub-daily time step for the UEB is necessary for accurate energy

balance calculation, even though the rest of the VSMBn is forced by daily meteorological data. The UEB is run in hourly time steps using a separate meteorological input data in this study, while algorithms will be developed in the future to disintegrate daily data into hourly data (Johnson and Fitzpatrick, 1977; Patron and Logan, 1981). Evapotranspiration algorithm of the VSMBn is turned off while snow is on the ground (SWE > 1.0 mm) and sublimation is computed by the UEB. The UEB does not affect the soil energy and water balance calculation when no snow is on the ground or falling, even though it still runs in the background.

3.3.2 Soil freezing and thawing

The VSMBo does not consider the phase change of soil water between ice and liquid, which severely restricts its ability to simulate snowmelt infiltration and runoff. A simple heat-conduction algorithm of Hayashi et al. (2007) is adapted to the VSMBn to incorporate the effects of phase change. In this method, heat conduction from the snow surface to the top soil layer and between two adjacent soil layers (upper to lower) is given by

$$q_h = -\lambda \, \Delta_z T / \Delta z \qquad (10)$$

where q_h (W m^{-2}) is the soil heat flux, $\Delta_z T$ (°C) is the difference in temperature between adjacent soil layers (lower minus upper), Δz (m) is the distance between the centres of two layers, and λ (W m^{-1} K^{-1}) is the bulk thermal conductivity given by the thickness-weighted harmonic mean conductivity of two layers. Thermal conductivity of individual soil layer is calculated as a function of water content using the equation of de Vries (1963) as described by Hayashi et al. (2007), assuming that the thermal conductivity of water is approximated by the geometric mean of the conductivities of ice and liquid water (Farouki, 1981). The laboratory data of the Spy Hill soil sample under unfrozen condition show that conductivity is overestimated by de Vries (1963) equation (solid line in Fig. 11a) under moderate to dry condition. Therefore, the equation was modified by subtracting an empirical correction factor (dashed line in Fig. 11a) for the purpose of this study.

The effect of snowcover and surface vegetation is represented by including them in the bulk thermal resistance r_0 (W^{-1} m^2 K) between the air and the first soil layer as:

$$r_0 = r_v + d_s/\lambda_s + d_1/(2\lambda_1) \qquad (11)$$

where r_v (W^{-1} m^2 K) is the thermal resistance of the vegetation cover, λ_s is snow thermal conductivity, d_s (m) is snowpack thickness, and λ_1 is the bulk thermal conductivity of the first soil layer having thickness d_1 (m) (Fig. 8b). Thermal conduction below the bottom of the soil column is represented by setting a constant temperature (T_{btm}, °C) at an imaginary node located at a fixed depth (z_{btm}, m) below the penetration of seasonal temperature waves, and calculating the conduction flux between the lowest soil layer and the imaginary node using Eq. 10. In this study, T_{btm} = 5 °C and z_{btm} = 8 m are used, based on the mean annual soil temperature at 1.5 m depth and the theory of annual temperature wave propagation (e.g. Jury and Horton, 2004, p.191).

Some unfrozen water remains in the soil at sub-zero temperature, and a significant amount of unfrozen water co-exists with ice even at very low temperature, which is called residual unfrozen water (Stähli et al., 1996). The relationship between soil temperature T and unfrozen water content θ_u is called soil freezing characteristic (SFC) (Miller, 1980). The SFC of the Spy Hill soil sample has a sharp initial drop of θ_u, followed by a gradual transition to the residual value of 0.06 (Fig. 11b). Rigorous non-linear numerical models (e.g. Flerchinger and Saxton, 1989) use the thermodynamic Clapeyron equation and the water retention characteristics of unfrozen soil to represent the SFC (Spaans and Baker, 1996), but such an approach is computationally intensive.

A simpler binary SFC (solid line in Fig. 11b) with the residual unfrozen water content (θ_{ur}) as the single parameter is used in the VSMBn in the following manner.

The net heat flux ($\Delta_z q_h$) for the top soil layer is calculated using Eqs. 10 and 11.

$$\Delta_z q_h = q_{h0} - q_{h1} = \frac{T_a - T_1}{r_0} - \left(\frac{d_1}{2\lambda_1} + \frac{d_2}{2\lambda_2}\right)^{-1} \frac{T_1 - T_2}{d_1/2 + d_2/2} \quad (12)$$

where q_{h0} and q_{h1} are heat flux from the surface to the first layer and from the first to the second layer, respectively; T_a is air temperature; T_1 and T_2 are soil temperature in the first and second layer, respectively; d_1 and d_2 are the thickness of the two layers; and λ_1 and λ_2 are the thermal conductivity of the two layers. The $\Delta_z q_h$ computed in Eq. 12 is stored as sensible and latent heat

$$\Delta_z q_h = (\Delta_t T\, c_s + \Delta_t \theta_f\, \rho_w L_f) d \quad (13)$$

where $\Delta_t T$ (°C) and $\Delta_t \theta_f$ are change in soil temperature and volumetric frozen water content, respectively, with time, ρ_w (kg m^{-3}) is the density of water, L_f (J kg^{-1}) is the latent heat of fusion, d (m) is the layer thickness, and c_s (J m^{-3} K^{-1}) is the volumetric heat capacity of bulk soil. The c_s is determined from the heat capacity and volume fraction of individual soil phases (Hillel, 2004, p. 221). If the soil layer is completely frozen or thawed (i.e. $T \neq 0$ °C), $\Delta_z q_h$ is converted to sensible heat until T reaches 0 °C, and any residual is converted to latent heat. If the soil is already frozen ($T = 0$ °C), $\Delta_z q_h$ is first used for phase change of all available water above θ_{ur} and any residual is converted to sensible heat. Similar calculations are sequentially performed for lower soil layers. Preliminary simulations using daily time steps encountered numerical instability. Therefore, the daily time step is divided into four-hour time steps and air temperature and snowcover thickness are estimated by linear interpolation between the two daily values.

3.3.3 Runoff, infiltration, and soil water redistribution

A higher amount of runoff generally occurs over frozen soil than the same soil under unfrozen condition due to the reduction in soil hydraulic conductivity. Rigorous numerical models use unsaturated hydraulic conductivity functions (e.g. Campbell, 1974; van Genuchten 1980) with an impedance factor (Jame and Norum ,1980; Lundin, 1990) to represent the effects of frozen water on hydraulic conductivity and iteratively solve the non-linear Richards equation for water flow. However, such an approach is not applicable to the VSMB that calculates the water balance of conceptual soil layers. Therefore, runoff over frozen soil is calculated by the same Curve Number method used for unfrozen soil, but with modification to reflect the effects of frozen water content in a manner that is consistent with previous field studies reporting the strong influence of frozen water content (e.g. Stein and Kane, 1983; Gray et al., 1985). When the top soil layer is frozen (i.e. $T \leq 0$ °C), the curve number (CN) determined by total water content (see Appendix) is increased to a frozen value (CN_f) by

$$CN_f = CN\,(1 + \beta\, \theta_f / \theta_{sat}) \quad (14)$$

where β is a dimensionless coefficient, and θ_f and θ_{sat} are the frozen water content and porosity, respectively, of the top soil layer. Conceptually similar approaches were previously used in other soil water balance models (Schroeder et al., 1994; Puurveen, 1996; Neitsch et al., 2005). In addition to the modification by Eq. 14, the depth-weighting factor for the CN calculation (see Eq. A1 and A2 in Appendix) is modified. If the top soil layer is frozen, the weighting factor for the top layer is set to 1, and those for all other layers are set to 0, to reflect the strong influence of the top soil (Gray et al., 2001).

After runoff is subtracted, the reminder of water input is added to the top soil layer and allowed to accumulate until the soil layer is completely thawed or saturation is reached. The temperature of added water is initially equal to the current temperature of the top soil layer, and subsequently adjusted in the soil freezing and thawing algorithm. When the frozen soil becomes saturated in any soil layer, drainage to the next layer occurs up to a maximum allowable drainage flux (f_{lxm}, mm d^{-1}). This represents the effects of preferential flow through large air-filled pores in frozen soil (Stähli et al., 1996).

3.4 Model parameters and initial condition

The VSMBo and VSMBn in this study have six soil layers (see Table 5 for layer depths), and the model default values for permanent grass are used for plant root extraction coefficients and the drying curve representing the effects of soil moisture condition on actual evaporation (Hayashi et al., 2010). Soil water storage parameters (listed in Table 5) and hydraulic diffusivity were determined by Hayashi et al. (2010). The residual unfrozen water content (θ_{ur}) is set at the minimum observed value of θ_u during frozen periods for the soil layers that had moisture sensors, and θ_{ur} of the fourth layer is used for deeper layers (Table 5).

The total water content (θ) and temperature (T) for the first four soil layers are initialized using the observed values at the first day of simulation. The observed θ in the middle of soil layers (e.g. 0.1 m for the 0-0.2 m layer) is used to represent the layer-average θ for the first four soil layers. The average of the two observed T at the layer boundaries is used to represent the layer-average T for the first three layers, and the observed value at 1.0 m is used to represent the 0.8-1.2 m layer. The same method is used for the comparison of observed and simulated temperature in the Results. The initial θ of the fifth layer is assumed to be the same as the fourth layer, and is assumed to be 0.25 for the sixth layer (Hayashi et al., 2010). The initial T for the fifth and sixth layer is estimated by linearly extrapolating the temperature gradient between the 1.0 and 1.5 m sensors.

A trial-and-error model calibration was performed by adjusting several key parameters (listed in Table 6) within their physically reasonable ranges. The UEB uses aerodynamic roughness (z_0, m) and depth of active soil layer (D_e, m) as fitting parameters for turbulent flux and ground heat flux calculation, respectively; and snow density (ρ_s, kg m^{-3}) has a sensitive effect on simulated SWE. The soil freezing and thawing rates are sensitive to λ_s and r_v in Eq. 11, and snowmelt runoff is sensitive to the parameter β in Eq. 14. These parameters are manually adjusted to minimize the difference between observed and simulated SWE, θ_u, and T with respect to the root-mean-squared error (RMSE) and mean bias error (MBE). At the same time, the parameters are adjusted to minimize the difference between the simulated and observed seasonal total R_{off}.

3.5 Results

3.5.1 Snow processes

The winter period in this study is defined as a period from November 1 to May 15 based on the meteorological and soil conditions of the study site. Daily mean air temperature (T_m) and precipitation (P) of the three winters examined are shown in Figs. 12a, 13a, and 14a. Mean air temperature during the whole winter period was -1.8 °C in 2006-07, -2.9 °C in 2007-08, and -3.3 °C in 2008-09. The 1971-2000 normal mean temperature at the Calgary International Airport

(YYC) for this period is -2.8 °C (Environment Canada, 2011), suggesting that the winter of 2006-07 was warmer than normal. Total winter-period precipitation (uncorrected for wind under-catch) at YYC was 176 mm in 2006-07,104 mm in 2007-08, and 137 mm in 2008-09, where the normal precipitation at YYC is 115 mm (Environment Canada, 2011). Therefore, the amount of winter precipitation was above normal in 2006-07 and 2008-09, and below normal in 2007-08. This is reflected in the relative amount of precipitation (corrected for under-catch) at the study site in the three winters (Table 7).

All winter periods had strong mid-winter (i.e. January-February) Chinook events with T_m exceeding 5 °C. The Chinook event on January 16-19, 2009 was particularly strong with a four-day average T_m of 6.5 °C, which was followed by two more events on January 30 and February 3-5 (Fig. 14a). This happened after the main accumulation period, causing the almost complete depletion of snowpack (Fig. 14b), which is in contrast to the 2006-07 winter, in which the snowpack developed in February and persisted until the main snowmelt event in March (Fig. 12b).

Turbulent heat fluxes during Chinook events can be examined using the eddy-covariance data. However, eddy-covariance systems almost always underestimate turbulent fluxes (Wilson et al., 2002), resulting in the incorrect energy balance between $L_vF_v + H$ and $R_n - Q_g$, where L_v (J kg^{-1}) is the latent heat of vaporization, F_v (kg m^{-2} s^{-1}) and H (W m^{-2}) are vapour and sensible heat fluxes, respectively, directed to the atmosphere, R_n (W m^{-2}) is net radiation, and Q_g (W m^{-2}) is downward ground heat flux. In this study, the energy balance correction was made with the Bowen ratio method of Twine et al. (2000), using the procedure described by Hayashi et al. (2010), for those days with no snowcover. However, it is impossible to make the same energy-balance correction in other days because the latent heat associated with snowmelt and refreezing cannot be measured accurately. To estimate the degree of flux underestimation, daily average $L_vF_v + H$ and $R_n - Q_g$ are plotted in Fig. 15 for those days during the three winters that had little or no snow on the ground and had sufficiently large magnitudes (> 30 W m^{-2}) of $L_vF_v + H$ and $R_n - Q_g$ to reduce the scatter caused by low single-to-noise ratio. The slope of 0.752 in the plot indicates the degree of turbulent flux underestimation. Hayashi et al. (2010) obtained similar results for May-October data at the same study site and showed that making a full energy balance correction resulted in unrealistically high values of F_v. They suggested using the arithmetic average value between the raw and energy-balance-corrected F_v as a reasonable estimate of true F_v. In this study, the raw F_v data on those days with snow on the ground are divided by 0.88, which is the average of full correction (0.752) and no correction (1), to estimate F_v.

The estimated daily average vapour flux is plotted using the unit of (mm d^{-1}) in Fig. 12c, 13c, and 14c for those days that had at least 45 of 48 half-hourly data points. Note that the humidity sensor in the eddy-covariance system failed to function during some precipitation events, resulting in data gaps. The vapour flux was generally less than 0.5 mm d^{-1}, but high flux values exceeding 1.4 mm d^{-1} occurred during strong Chinook events, for example, on January 16-18 and January 27-30, 2009 (Fig. 14c).

The VSMBo overestimated snow accumulation in all three winters (Figs. 12b, 13b, and 14b) and failed to simulate snowpack depletion during the mid-winter Chinook event in 2008-09 (Fig. 14b). Snow algorithms of the VSMBn were calibrated by adjusting z_0, ρ_s, and D_e (Table 6). The calibrated z_0 (= 1 mm) is within the commonly reported range of 1-5 mm (e.g. Moore 1983). Compared to the calibrated ρ_s (= 190 kg m^{-3}), the average and standard deviation of all snow density measurements (n = 37) at the study site was 184 ± 51 kg m^{-3}. The RMSE and MBE of calibrated VSMBn are listed in Table 4.

3.5.2 Soil temperature and moisture

Observed soil temperature at 0.1 m depth reached 0 °C in mid to late November in all three winters, indicating the arrival of the freezing front (Figs. 12d, 13d, and 14d), which roughly coincided with a sharp decrease of the amount of unfrozen water in the top 0.4 m of soil (Figs. 12e, 13e, 14e). The freezing front reached a depth of 1.0 m on February 4 in the 2006-07 winter, January 15 in 2007-08, and February 22 in 2008-09 (Figs. 12d, 13d, and 14d). The freezing front did not reach the deepest temperature sensor (1.5 m) in all three winters (data not shown). The spring thawing of soil at 0.1 m started on March 18 in 2006-07, April 8 in 2007-08, and March 18 in 2008-09 as indicated by a gradual increase in the amount of unfrozen water in the top 0.4 m of soil (Figs. 12e, 13e, and 14e) and steady values of T at 0 °C (Figs. 12d, 13d, and 14d). Mid-winter Chinook events caused partial thawing of the top soil, particularly during the strong Chinook event on January 16-19, 2009 (Fig. 12d,e). The T at 0.1 m remained near 0 °C for an extended time period in all three winters reflecting the complex effects of snowmelt and the partial thawing and refreezing of soil water. The thawing also occurred from the bottom of the frozen layer and the upward-moving thawing front reached 1.0 m in early to mid March (Fig. 12d, 13d, and 14d). The two thawing fronts met at depths of 0.4-0.6 m (data not shown) and the complete thawing of the entire soil column occurred around April 20 in 2006-07, April 16 in 2007-08, and April 19 in 2008-09.

The soil surface temperature estimated by the VSMBo is very sensitive to air temperature (see Eq. 7). This resulted in the simulated thawing of the top soil that was much earlier than the observation in all three winters (Figs. 12d, 13d, and 14d). Soil freezing and thawing algorithms of the VSMBn was calibrated by adjusting r_v (Table 6), whereas λ_s was calculated from the calibrated value of ρ_s using Eq. 63 of Jordan (1991). The calibrated VSMBn simulated a higher amplitude of temperature fluctuations than observed, due to the binary approximation of smooth SFC (Fig. 11b), but it tracked the overall temperature trends reasonably well and predicted the complete thawing of the top soil layer within 3-5 days of actual dates (Figs. 12d, 13d, and 14d). The simulated T by the VSMBn had RMSE and MBE in ranges of 0.8 to 1.9 °C and -0.4 to 0.4 °C, respectively, for the first four soil layers, where the observation data were available (Table 8).

The VSMBn tended to overestimate the amount of unfrozen water in the top 0.4 m of soil and underestimate it in the 0.4-1.2 m zone (Fig. 12e, 13e, and 14e) because the soil freezing-thawing algorithm keeps unfrozen water in frozen soil layers until saturation is reached. The simulated unfrozen water content in the first four layers had RMSE and MBE in ranges of 0.003 to 0.063 and -0.011 to 0.024, respectively (Table 8), with shallower soil layers having relatively high magnitude of errors.

3.5.3 Snowmelt runoff

The snowmelt runoff started to fill the depression during the spring melt event on March 7, 2007 and generated a total estimated runoff of 14.3 mm averaged over the catchment (Fig. 12f). No snowmelt runoff was observed in the depression in 2007-08 (Fig. 13f), presumably as a result of lower amount of precipitation than other winters (Table 7). The mid-winter Chinook event in January 2009 caused no snowmelt runoff to reach the depression (Fig. 14f), while almost completely depleting the snowpack (Fig. 14b). Only 1.2 mm of runoff was observed in 2008-09 (Fig. 14f). The runoff in 2008-09 was an order of magnitude smaller than in 2006-07, even

though the two winters had similar amounts of precipitation (Table 7). Some part of the difference may be due to the method of using a depression to estimate runoff, which ignores the initial infiltration of runoff water into the depression soil. This may cause underestimation of runoff, which has more pronounced effects on low runoff years (i.e. 2008-09) than high runoff years. The observed difference, however, should reflect the true difference in runoff amounts between the two winters because the water level records and visual observation from other depressions in the area clearly indicated the larger magnitude of snowmelt runoff in 2006-07 than in 2008-09.

The VSMBo substantially overestimated total snowmelt runoff in 2006-07 and 2007-08, and slightly underestimated it in 2008-09 (Figs. 12f, 13f, 14f; Table 9). The snowmelt runoff algorithm of the VSMBn was calibrated by adjusting β (Table 6), while f_{lxm} was set to 10 mm d^{-1} based on van Dijk (2005), who monitored snowmelt infiltration rates through frozen soil under several ponds in the Spy Hill area. The calibrated VSMBn estimated the total amount of snowmelt runoff reasonably close to the observed value in 2006-07 (Fig. 12f, Table 9), and a very small value in 2007-08, consistent with observation (Fig. 13f, Table 9). The VSMBn overestimated the observed total snowmelt runoff in 2008-09 (Fig. 14f, Table 9), even though it captured the relative magnitude of runoff among the three years.

3.5.4 Water balance

The VSMBn calculates the water balance of snowpack for each time step as

$$\Delta SWE = P - M - E_s \quad (15)$$

where ΔSWE (mm) is the change in SWE, P (mm) is precipitation, M (mm) is the amount of melt water drainage, and E_s (mm) is sublimation calculated by the energy balance. When there is no snow on the ground, the model simply passes the rainfall through a "transparent" snowpack, and treats it as part of M. The VSMBo keeps track of SWE using the same approach, but E_s is accounted for by the initial 30 % loss of P and evaporation at the potential rate when daily net radiation is positive. The seasonal total M calculated by the VSMBo was smaller than the value simulated by the VSMBn in 2006-07 and 2007-08, and slightly larger in 2008-09 (Table 7). The contrast between the first two winters and the last winter is related to the higher total E_s calculated by the VSMBn than the VSMBo in 2008-09 (Table 5), in which the VSMBo did not correctly simulate the snowpack depletion during the major Chinook event on January 16-19 (Fig. 14b).

The water balance of the entire soil column in the two models is

$$\Delta S = M - E - R_{off} - G \quad (16)$$

where ΔS (mm) is change in the total amount of water in the soil column, E (mm) is evapotranspiration, and G (mm) is the amount of drainage from the bottom of soil column. Based on the low hydraulic conductivity of glacial till at depths below 3 m in the study area (van Dijk, 2005) and very stable values of observed θ at 1.0 m (data not shown), G is assumed negligible for the time scale of one winter. For the entire winter period starting and ending with no snow (i.e. $\Delta SWE = 0$), substituting Eq. 15 into Eq. 16 gives

$$P - (E_s + E) - R_{off} - \Delta S = 0 \quad (17)$$

which can be used to evaluate the accuracy of field data with respect to the whole season water balance. To estimate the total observed $E_s + E$ for the entire winter period including the days with missing data, the sum of all available $E_s + E$ data for each winter was multiplied by a factor, f_{ec} = (total number of days) / (number of days with available data). The f_{ec} was 1.4 for 2006-07,

1.2 for 2007-08, and 1.3 for 2008-09. The soil water storage change, ΔS was estimated for the top four soil layers by multiplying the observed volumetric water content by layer thickness. The bottom two layers (1.2-2.0 and 2.0-4.0 m) were excluded from the calculation because no data were available.

The observed water balance data show that 50-60 % of precipitation returns to the atmosphere as E_s and E (Table 9). Of the remainder of P, the majority infiltrates and a small fraction becomes surface runoff (Table 9). The water balance (Eq. 17) is not perfectly closed for the field data (i.e. the sum of all terms in the left hand side is not equal to zero), reflecting the uncertainty and errors in measuring and estimating individual components on the left hand side. The magnitude of water balance residual, W_{res} (mm) was 11-30 mm, or 6-22 % of P (Table 9), which is comparable to the magnitude of errors reported in previous water-balance studies of frozen soil (e.g. Bayard et al. 2005; Iwata et al., 2010). Potential sources of errors in turbulent flux measurement and the estimation of R_{off} using the depression as a collector have been discussed above. The uncertainty in ΔS results from using a single site to represent the soil moisture condition of a larger area, and also from instrumental errors. The RMSE of the calibration of the capacitance soil moisture sensor was in the order of 0.01 to 0.03 by volumetric water content (Hayashi et al., 2010), which is equivalent to 12-36 mm for a 1.2 m deep soil column. Despite these uncertainties, the values listed in Table 5 provide reasonable estimates of water balance components for model evaluation, with an error magnitude in the order of 30 mm. Comparing the water balance components estimated from observed data and simulated by the two models (Table 9), simulated values are generally within 30 mm of the observed values. The maximum deviation from the observed values was -33.7 mm for the VSMBn-simulated $E_s + E$ in 2006-07.

3.6 Concluding remarks on implementation of winter processes

The new VSMB simulates the snow processes more accurately than the old model, particularly for mid-winter Chinook events that cause major depletion of snowpack, thereby affecting the soil water balance and snowmelt runoff. The simple soil freezing and thawing algorithm in the new VSMB estimates the date of thawing within a few days of observed dates, and the snowmelt runoff algorithm estimates the amount of total runoff within a few millimeters of observed values. However, the model still has limitations in accurately predicting the vertical distribution of water content during the thawing period.

The new model will expand the capability of the VSMB to whole-year application including winter periods, which will be useful for predicting the pre-seeding soil moisture condition and estimating the amount of snowmelt runoff, which fills water reservoirs and natural depressions and wetlands. Since the new VSMB has only been tested at a single site that has heavy-textured soil and permanent grass cover, it is important to test the model under different soil, landuse, and climatic conditions. The future efforts are also required to disintegrate daily meteorological data into shorter (e.g. hourly) intervals, so that daily data set can be used to force the snow energy balance algorithm in the VSMB.

3.7 Appendix: NRCS Curve Number method

Akinremi et al. (1996) modified the standard Curve Number method to compute the dimensionless curve number (*CN*) using two dimensionless parameters, c_d and c_w, reflecting the moisture condition of all soil layers

$$c_d = \sum_{i=1}^{n} [wf_i \times (\theta_i - \theta_{WPi}) / (\theta_{FCi} - \theta_{WPi})] \quad \text{(A1)}$$

$$c_w = \sum_{i=1}^{n} (wf_i \times \theta_i / \theta_{FCi}) \quad \text{(A2)}$$

where wf_i is a depth weighting factor the i-th soil layer, with i increasing from 1 at the top and n at the bottom, θ is total volumetric water content, and θ_{FC} and θ_{WP} are the volumetric water content at field capacity and wilting point, respectively. The weighting factor is specified by an exponential function, which takes the maximum value at the soil surface and becomes negligible (< 0.01) at a depth of 0.5 m. The *CN* is given by:

$$CN = CN_1 + c_d (CN_2 - CN_1) \qquad c_d < 1 \quad \text{(A3)}$$

$$CN = CN_2 + c_w (CN_3 - CN_2) \qquad c_d \geq 1 \quad \text{(A4)}$$

where CN_2 is the "master" curve number dependent on soil type, landcover, and agricultural practices; and CN_1 and CN_3 are computed from CN_2 by

$$CN_1 = CN_2 - 20 \times (100 - CN_2) / [100 - CN_2 + \exp\{2.533 - 0.063(100 - CN_2)\}] \quad \text{(A5)}$$

$$CN_3 = CN_2 \exp[0.006729(100 - CN_2)] \quad \text{(A6)}$$

The VSMBo uses a default value of $CN_2 = 80$ representing the condition of the Agriculture and Agri-Food Canada research stations at Swift Current, Saskatchewan and Lethbridge, Alberta, where the model was developed and tested (Akinremi et al. 1996). The maximum allowed value of CN_1 is 0.4 CN_2. If the computed value of CN_1 is greater than $0.4CN_2$, it is set at $0.4CN_2$. From the calculated value of *CN*, R_{off} (mm) is given by:

$$S = 254 (100 - CN) / CN \quad \text{(A7)}$$

$$R_{off} = (W_{in} - 0.2S)^2 / (W_{in} + 0.8S) \quad \text{if } W_{in} > 0.2S \quad \text{(A8)}$$

$$= 0 \quad \text{if } W_{in} \leq 0.2S$$

where S (mm) is a retention parameter representing the effects of soil and plant canopy. When Eq. A2 is applied to frozen soil, in which θ_i (sum of frozen and unfrozen water) may exceed θ_{FCi} for an extended time period, the value of c_w is capped at 1.

Table 5 Soil water storage parameters used in the VSMB: volumetric water content at saturation (θ_{sat}), field capacity (θ_{FC}), and wilting point (θ_{WP}); and the residual unfrozen water content (θ_{ur}) in frozen soil.

Depth (m)	θ_{sat}	θ_{FC}	θ_{WP}	θ_{ur}
0-0.2	0.53	0.32	0.12	0.10
0.2-0.4	0.55	0.37	0.14	0.12
0.4-0.8	0.53	0.38	0.18	0.19
0.8-1.2	0.46	0.38	0.18	0.18
1.2-2.0	0.46	0.38	0.18	0.18
2.0-4.0	0.46	0.38	0.18	0.18

Table 6 Calibrated parameter values used in the VSMBn.

Parameter	Description	Calibrated value
z_0	Surface aerodynamic roughness	1.0 mm
ρ_s	Snow density	190 kg m^{-3}
D_e	Depth of active soil layer in the UEB snow algorithm	0.1 m
λ_s	Bulk thermal conductivity of snow	0.15 W m^{-1} K^{-1}
r_v	Bulk thermal vegetation resistance	0.2 W^{-1} m^2 K
β	Frozen soil runoff parameter (Eq. 7)	0.02
f_{lxm}	Maximum allowable drainage for saturated-frozen soil	10 mm d^{-1}

Table 7 Summary of the observed precipitation (P), drainage from snowpack (M), and the sublimation (E_s) estimated by the VSMB for the three winter periods (November 1 - May 15).

	P (mm)			M (mm)		E_s (mm)	
Year	Snow	Rain	Total	VSMBo	VSMBn	VSMBo	VSMBn
2006-07	143.0	70.9	213.9	169.1	183.8	43.6	31.1
2007-08	125.0	12.9	137.9	97.0	113.7	40.9	25.3
2008-09	156.4	37.6	194.0	146.2	141.5	47.5	53.5

Table 8 The root-mean-squared error (RMSE) and mean bias error (MBE) of the calibrated VSMBn. Soil variables are unfrozen water content (θ_u) and temperature (T), where the statistics are calculated using all daily data points. The statics of snow water equivalent (SWE) is calculated using the indicated number (n) of data points.

	Depth	θ_u		T (°C)		SWE (mm)		
Year	(m)	RMSE	MBE	RMSE	MBE	n	RMSE	MBE
2006-07	0.1	0.063	0.024	1.3	-0.1	33	5.0	0.8
	0.3	0.055	0.021	1.1	-0.2			
	0.6	0.022	0.003	1.0	-0.1			
	1.0	0.019	0.001	0.9	0.4			
2007-08	0.1	0.029	0.011	1.9	-0.4	5	5.0	-4.6
	0.3	0.032	0.001	1.6	-0.3			
	0.6	0.003	0.001	1.0	0.0			
	1.0	0.015	0.014	0.8	0.3			
2008-09	0.1	0.047	0.025	1.7	-0.1	13	7.2	0.5
	0.3	0.039	0.017	1.3	-0.1			
	0.6	0.022	-0.011	0.9	0.1			
	1.0	0.032	-0.010	0.8	0.4			

Table 9 Total soil water balance components for the three winter periods: Precipitation (P), sublimation and evapotranspiration ($E_s + E$), soil water storage change (ΔS), runoff (R_{off}), and water balance residual (W_{res}).

	Field observation					VSMBo simulation			VSMBn simulation		
	P	$E_s + E$	ΔS	R_{off}	W_{res}	$E_s + E$	ΔS	R_{off}	$E_s + E$	ΔS	R_{off}
Year	(mm)	(mm)	(mm)	(mm)	(mm)	(mm)	(mm)	(mm)	(mm)	(mm)	(mm)
2006-07	213.9	127.2	97.3	14.1	-26.9	107.8	71.4	34.7	93.5	106.0	14.3
2007-08	137.9	76.2	29.9	0.0	30.2	86.0	39.2	12.7	80.5	56.9	0.5
2008-09	194.0	95.2	106.5	1.2	-10.8	107.2	86.5	0.3	99.2	87.5	7.3

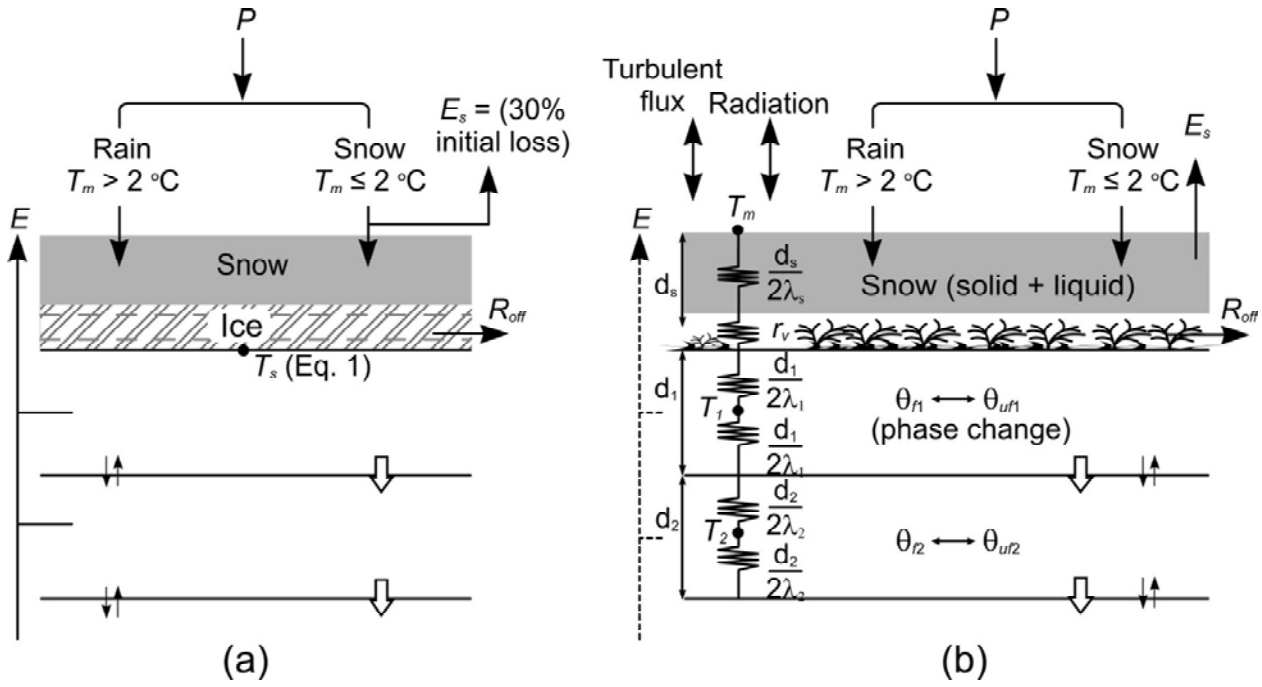

Fig. 8 Schematic diagrams of winter processes in (a) the old VSMB model and (b) the new VSMB model modified in this study. The symbols and processes are explained in the texts.

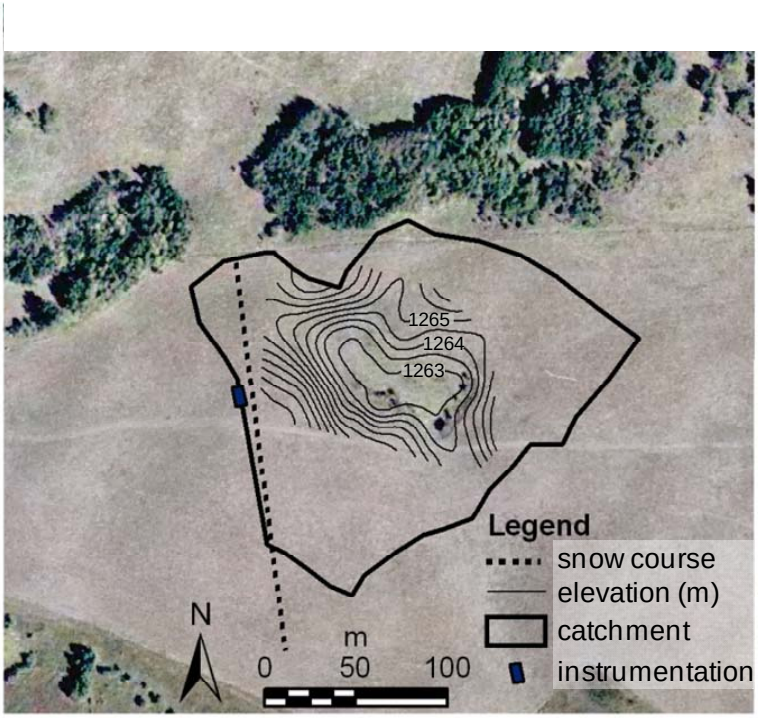

Fig. 9 Aerial photograph of the Spy Hill site showing the location of instrumented site, snow survey course, and the extent of the catchment draining to a depression. Elevation contours are derived from detailed survey data (Jackson 2008) and drawn at 0.5 m interval.

Fig. 10 Photographs of Spy Hill site (December 2009). Top: eddy-covariance energy balance system. Bottom: snow density measurement using a aluminum sampling tube.

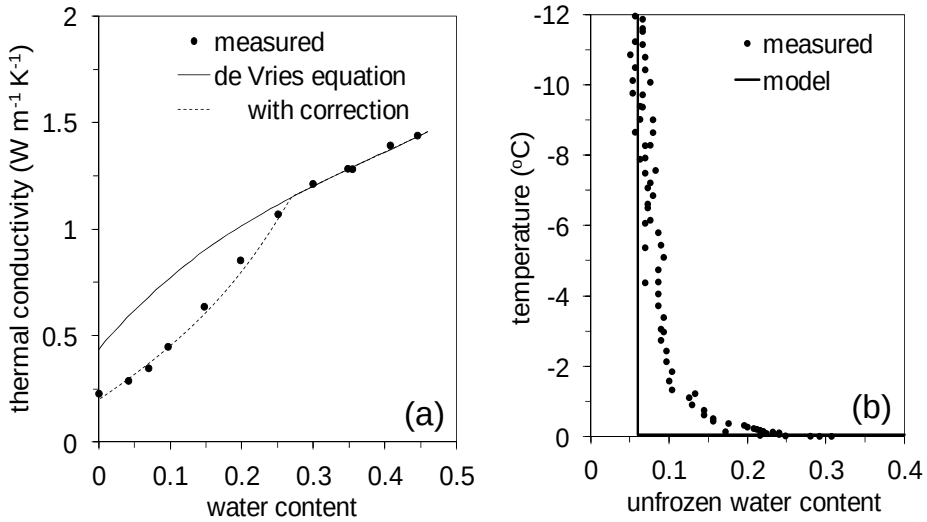

Fig. 11 (a) Thermal conductivity of an unfrozen soil sample collected from the instrumented site. Solid circles indicate laboratory measurements and lines indicate conductivity models. (b) Soil freezing characteristics of the same soil sample. Solid circles indicate laboratory measurements and the solid line indicates the binary approximation used in the VSMBn.

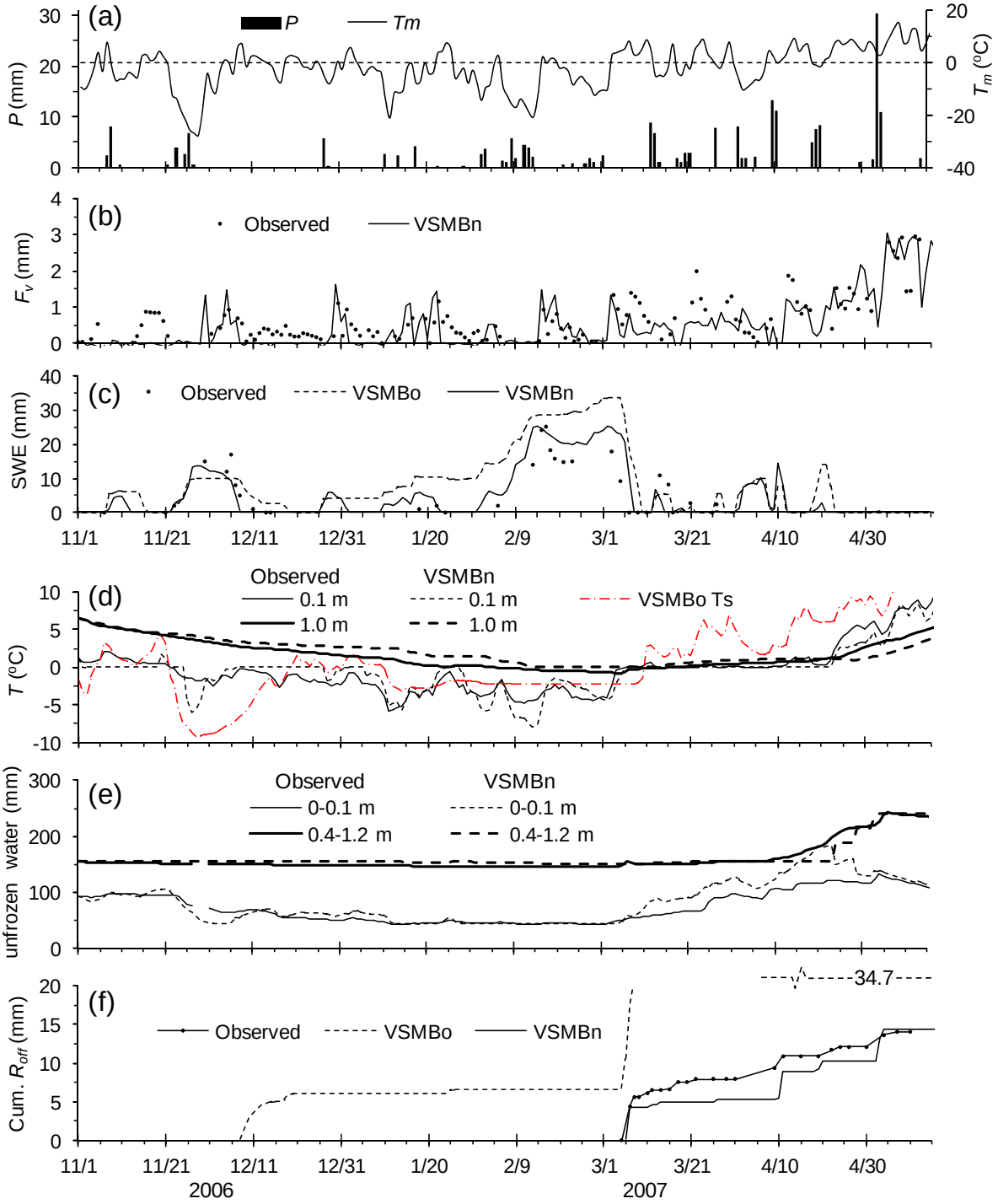

Fig. 12 The results for the winter 2006-07. (a) Observed mean daily air temperature (T_m) and daily precipitation (P). Dashed line indicates 0 °C. (b) Observed and VSMBn-simulated vapour flux (F_v). (c) Observed and simulated snow water equivalent (SWE). (d) Observed and VSMBn-simulated soil temperature at 0.1- and 1.0-m depths, and VSMBo-simulated soil surface temperature (T_s). (e) Observed and simulated amount of unfrozen water in the first and second soil layers (0-0.4 m) and the third and fourth layers (0.4-1.2 m). (f) Observed and simulated cumulative runoff (R_{off}). Note that VSMBo-simulated R_{off} is out of scale.

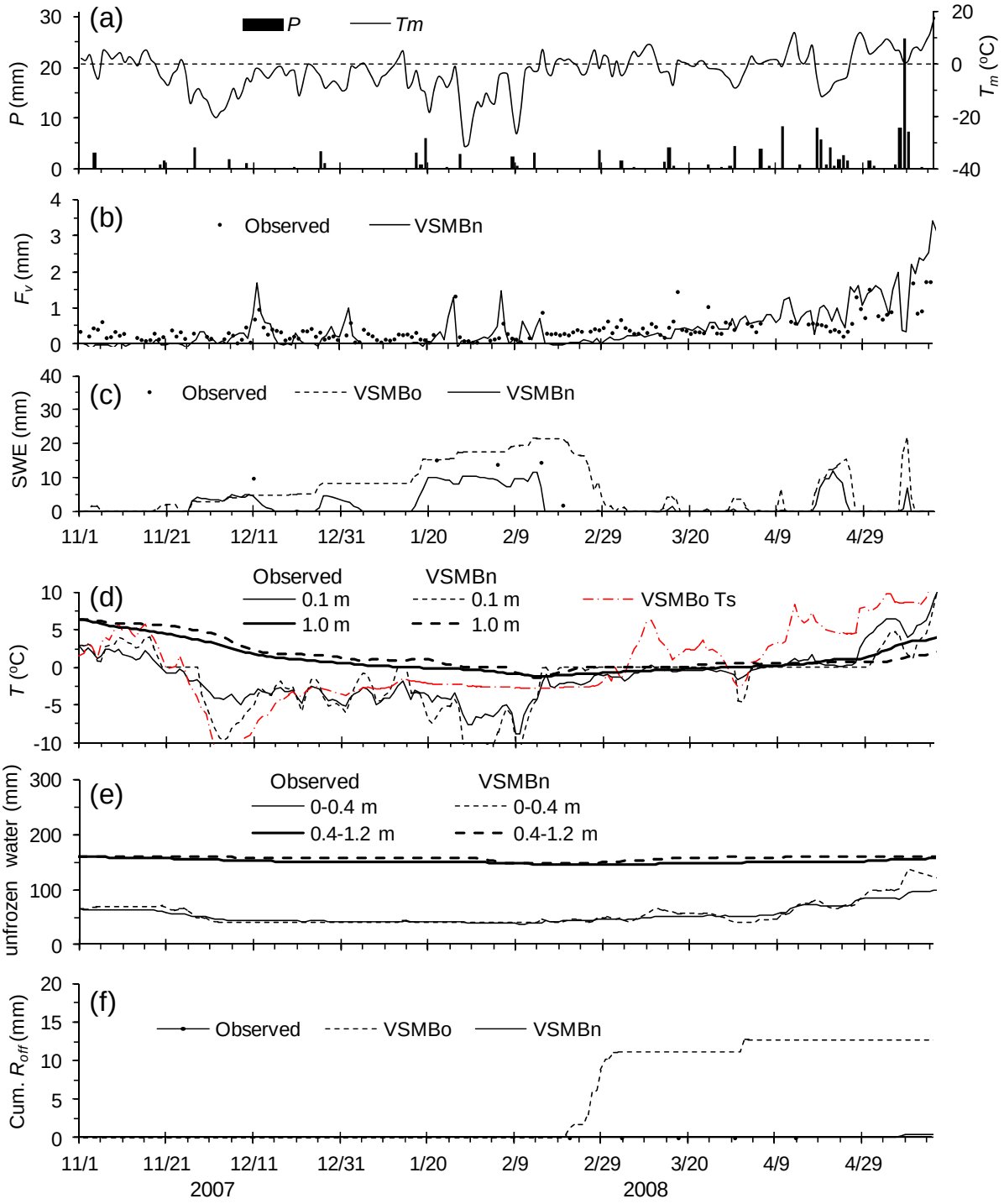

Fig. 13 The results for the winter 2007-08. (a) Observed mean daily air temperature (T_m) and daily precipitation (P). (b) Observed and VSMBn-simulated vapour flux (F_v). (c) Observed and simulated snow water equivalent (SWE). (d) Observed and VSMBn-simulated soil temperature at 0.1- and 1.0-m depths, and VSMBo-simulated soil surface temperature (T_s). (e) Observed and simulated amount of unfrozen water in the first and second soil layers (0-0.4 m) and the third and fourth layers (0.4-1.2 m). (f) Observed and simulated cumulative runoff (R_{off}).

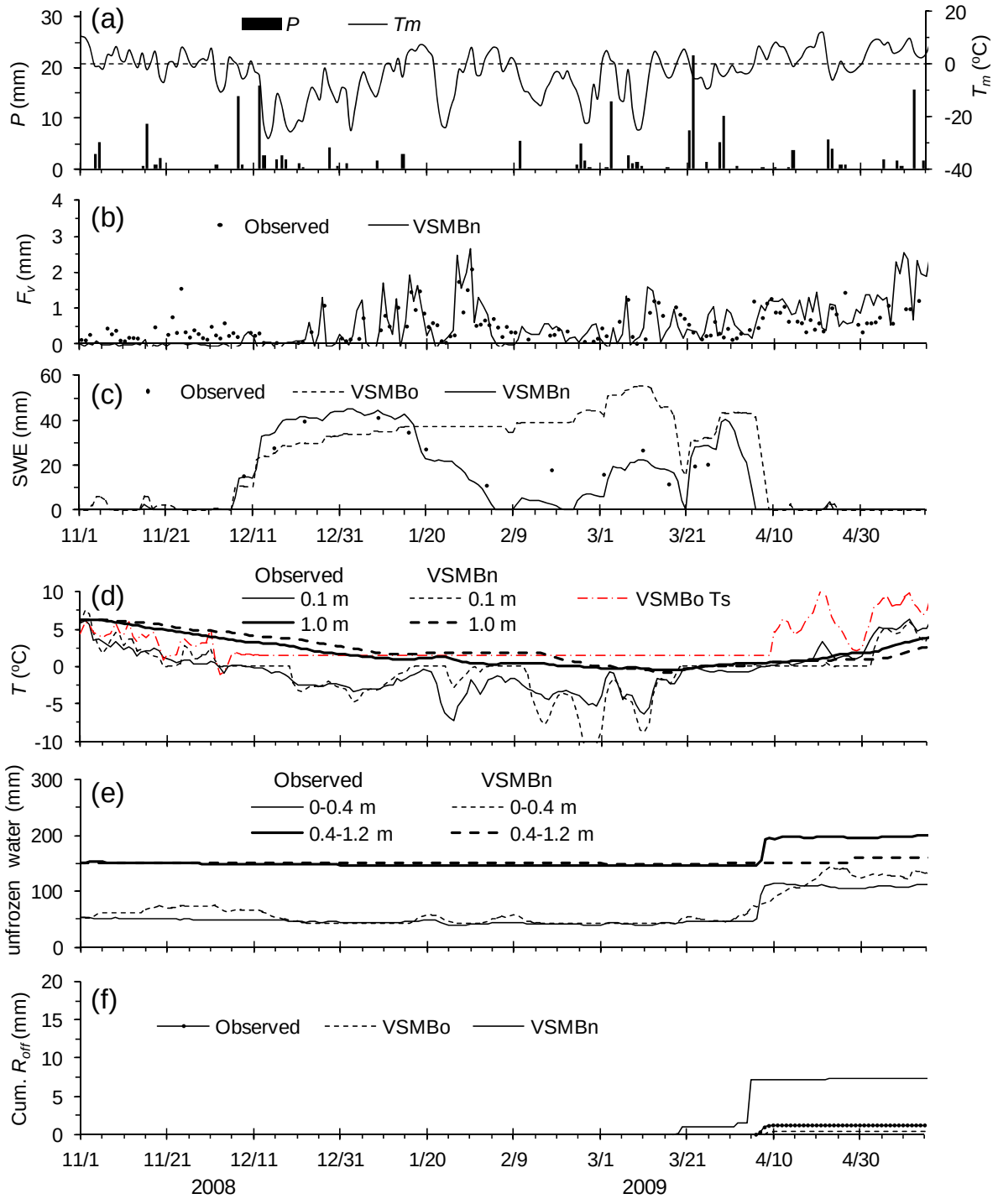

Fig. 14 The results for the winter 2007-08. (a) Observed mean daily air temperature (T_m) and daily precipitation (P). (b) Observed and VSMBn-simulated vapour flux (F_v). (c) Observed and simulated snow water equivalent (SWE). (d) Observed and VSMBn-simulated soil temperature at 0.1- and 1.0-m depths, and VSMBo-simulated soil surface temperature (T_s). (e) Observed and simulated amount of unfrozen water in the first and second soil layers (0-0.4 m) and the third and fourth layers (0.4-1.2 m). (f) Observed and simulated cumulative runoff (R_{off}).

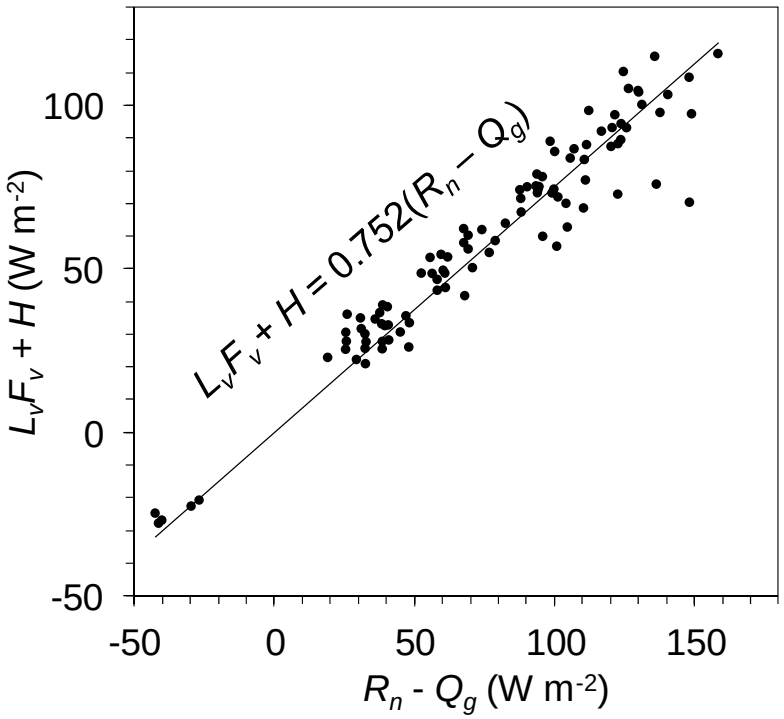

Fig. 15 Cross plot of daily average latent (L_vF_v) plus sensible (H) heat flux and net radiation (R_n) minus ground heat flux (Q_g), measured at the instrumented site for days with little or no snow on the ground during the winter periods of 2006-09. The solid line shows the least-squares regression.

4 Determination of VSMB water retention parameters for prairie soils

4.1 Background information

The VSMB uses field capacity and wilting point to specify the soil water retention capacity. The volumetric water content at field capacity (θ_{FC}) and wilting point (θ_{WP}) can be determined *in situ* if the soil water content is monitored continuously in the field (see Section 2.3). In absence of such data, θ_{FC} and θ_{WP} need to be estimated from the soil texture using pedo-transfer functions (PTF) approach (e.g. Schaap et al., 2001). The PTF approach has become popular in the past decade, but its applicability to the soils in Alberta and the degree of errors and uncertainty has not been evaluated. The objective of this part of study is to determine θ_{FC}, θ_{WP}, and saturated hydraulic conductivity (K_{sat}, m s^{-1}) of the soil samples collected from the six sites (Fig. 1) and examine the relationship between these hydraulic parameters and soil texture.

4.2 Study sites and methods

Six sampling sites are all located adjacent to existing meteorological stations, and were selected to represent typical medium-texture soils of Alberta and to cover a relatively large geographical area in the Prairies region of southern Alberta (Fig. 1). Soil samples were collected from four depths at each location (five at Rosemary) using 100 cm^3 stainless-steel soil rings. Duplicate samples were collected from each depth. To collect the samples, a pit was dug into the soil, and one of the side walls of the pit was cleaned to observe soil profiles. Based on the observation, the depths of samples were selected to represent major soil horizons. A horizontal surface of the soil was exposed at the shallowest sampling depth and a soil ring was hammered in vertically (Fig. 16). The soil ring was subsequently retrieved by carefully removing the soil around the ring. The second sample was collected from the same depth, and the procedure was repeated at deeper sampling depths.

The sample rings were sealed with plastic caps, placed in a sealable bag, and transported to the laboratory. The samples were weighed using an electronic balance with 0.1 g precision within a day or two of sampling, and stored in a refrigerator. One of the two samples from each location and depth was analyzed for K_{sat} using the falling-head permeameter method (Reynolds and Elrick, 2002). After the analysis, the sample was weighed to determine the saturated weight, and subsequently oven-dried at 105 °C for 48 hours to determine the dry weight. The porosity of samples was calculated from the difference between saturated and dry weight, and bulk density from the dry weight. The samples were pulverized using an anvil and sieved into > 2 mm, 1-2 mm, and < 1 mm size fractions; and the weight of each fraction were determined. The < 1 mm fraction was put through a sifter several times until a sample of *ca*. 0.5-0.8 g was obtained. These samples were put through the Mastersizer laser diffractor to determine the grain size distribution (Gee and Or, 2002). The soil texture of each sample was determined using the results of sieve analysis and laser diffractor analysis.

The second set of samples was subjected to the analysis of soil water retention characteristics using the pressure-plate extractor method (Dane and Hopmans, 2002). The top 2-2.5 cm of soil in the 5 cm high sample ring was removed to decrease the thickness of sample and shorten the equilibration time for each step of pressure. The volume of removed soil was estimated by measuring the vertical distance between the top of the sample ring and the soil surface at four

locations along the ring and taking the average. The bottom of the sample was covered by a filter cloth and the samples were saturated by placing them in a tub of de-aired water for two days. The samples were quickly removed from the tub and weighed before the water was drained from the soil to determine the saturated weight. They were subsequently placed on a porous ceramic plate and kept in the pressure chamber under ambient pressure for two days to allow drainage, and weighed. The tension head (i.e. the magnitude of matric potential head) at this stage was assumed to be half the height of soil sample (*ca*. 0.01 m). The pressure in the system was increased in steps to achieve the tension head of 0.1 m, 0.2 m, 0.4 m, 0.8 m, 2 m, 4 m, 8 m, 20 m, and 40 m; and the samples were weighed at each step of tension head. The equilibration time was increased from two days for the first step to 25 days for the last step. After the last step, the samples were oven-dried at 105 °C for 48 hours and weighed. Volumetric water content at each stage was determined from the difference in weight and the volume of sample.

The measured data of tension head and volumetric water content were plotted on a graph for each sample, and the van Genuchten (1980) equation was use to fit a smooth curve for the water retention characteristics:

$$S_e = (\theta - \theta_r) / (\theta_s - \theta_r) = 1 / [1 + (-\alpha\psi_m)^n]^{1-1/n} \quad (18)$$

where S_e is effective saturation, θ is volumetric water content, θ_s is saturation water content, θ_r is residual water content, α (m^{-1}) is a parameter representing the reciprocal of capillary length, ψ_m (m) is matric potential head, and n is a parameter representing the degree of sorting of grains. Three parameters (θ_r, α, n) were used as fitting parameters to be determined by the least-squares regression technique. To prevent unrealistically low or high values of θ_r, its values were constrained between 0.03 and 0.l. Once the coefficients for Eq. (18) have been determined, θ_{FC} was calculated from Eq. (18) as the value of θ at ψ_m = -1 m, and θ_{WP} as the value of θ at ψ_m = -150 m.

4.3 Results

Grain size distribution and soil texture class were determined for 25 samples (Rosemary site had five samples and other sites had four samples each). The samples from Neir, Beiseker, Morrin, and Iron Spring had medium to medium-coarse textures (Fig. 17). The samples from Barnwell and Rosemary had sandy texture (Fig. 17).

The K_{sat} of the 25 samples ranged from 2.6×10^{-6} to 2.7×10^{-3} m s^{-1} (Fig. 18). There was no obvious correlation between K_{sat} with clay fraction (Fig. 18a) or sand fraction (Fig. 18b) of the samples, except that the Morrin sample from a depth of 0.7 m had a high clay fraction (47 %) and low K_{sat}. The majority (92 %) of samples had K_{sat} between 10^{-4} and $10^{-2.5}$ m s^{-1} (Fig. 18c), suggesting that the VSMB may not be strongly affected by the variability in K_{sat} (and soil hydraulic diffusivity), except for the soils with very high clay fraction.

The water retention characteristics of most of the soil samples had a sharp drop in water content from the saturation to the first step of tension (0.01 m), as shown in an example of the Neir sample from a depth of 0.1 m (Fig. 19a). This is most likely attributed to the initial swelling of soil upon saturation (which does not occur under natural condition) and the drainage of macro pores between saturation and the lowest tension. In order to analyze the water retention characteristics of the soil matrix, the van Genuchten equation (Eq. 18) was fitted to the tension range between 0.01 m and 40 m, and the values of θ_{FC} and θ_{WP} were calculated (Fig. 19).

Estimated values of θ_{FC} ranged between 0.20 and 0.52, and θ_{WP} between 0.08 and 0.30 (Fig. 20a). Some of these values in higher end of the histogram appear unrealistically high for the

medium textured soil. Likely cause of overestimation is the error in the definition of soil volume. This issue will be resolved as the data are further refined and re-analyzed over the next few months. Using the estimated values of θ_{FC} and θ_{WP} in Fig. 20a, available water content ($\theta_{FC} - \theta_{WP}$) was computed for all samples (Fig. 20b). The values ranged between 0.08 and 0.32 with a mean of 0.20.

The θ_{FC} and θ_{WP} both had a weak negative correlation with sand fraction (Fig. 21a) and a weak positive correlation with clay fraction (Fig. 21b). The degree of correlation may become stronger after the data are re-analyzed to resolve the issue of soil volume definition (see above). The correlation between of θ_{FC} and θ_{WP} and the soil texture suggest that the pedo-transfer function (PTF) approach may be useful for estimating these parameters. There was no obvious correlation between $\theta_{FC} - \theta_{WP}$ and sand fraction or clay fraction.

4.4 Concluding remarks on the soil sampling and analysis

Twenty-five soil samples were collected from six locations in southern Alberta (Fig. 1). Most of the soil samples had medium to coarse texture, representing a range of soils encountered in the region. Saturated hydraulic conductivity (K_{sat}) of most samples was in a relatively narrow range of 10^{-4} to $10^{-2.5}$ m s^{-1} (Fig. 18), suggesting that the moisture diffusion algorithm of the VSMB model is not likely sensitive to the variability of K_{sat}, except in soils with very high (> 40 %) clay fraction. Preliminary results of the analysis of soil water retention characteristics indicate wide ranges of water contents at field capacity (θ_{FC}) and wilting point (θ_{WP}) (Fig. 20). There appear to be significant correlation between these variables and soil texture (Fig. 21), suggesting that it may be possible to estimate water retention parameters from soil texture.

Fig. 16 Photographs demonstrating the collection of soil samples. Top: A sample ring is placed on a horizontal surface and hammered in. Bottom: The sample ring is retrieved by carefully removing the soil around the ring.

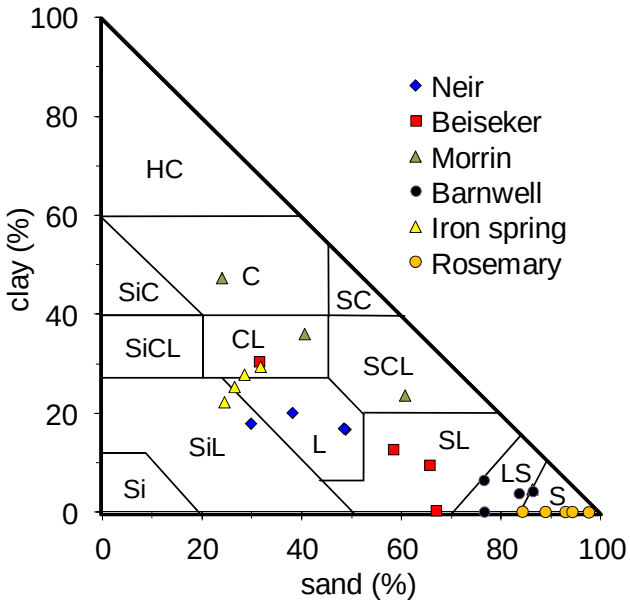

Fig. 17 Texture classes of the soil samples from the six sampling site. Abbreviations for the texture classes are HC, heavy clay; C, clay; SiC, silty clay; SiCL, silty clay loam; CL, clay loam; SC, sandy clay; SiL, silt loam; L, loam; SCL, sandy clay loam; SL, sandy loam; SI, silt; LS, loamy sand; S, sand.

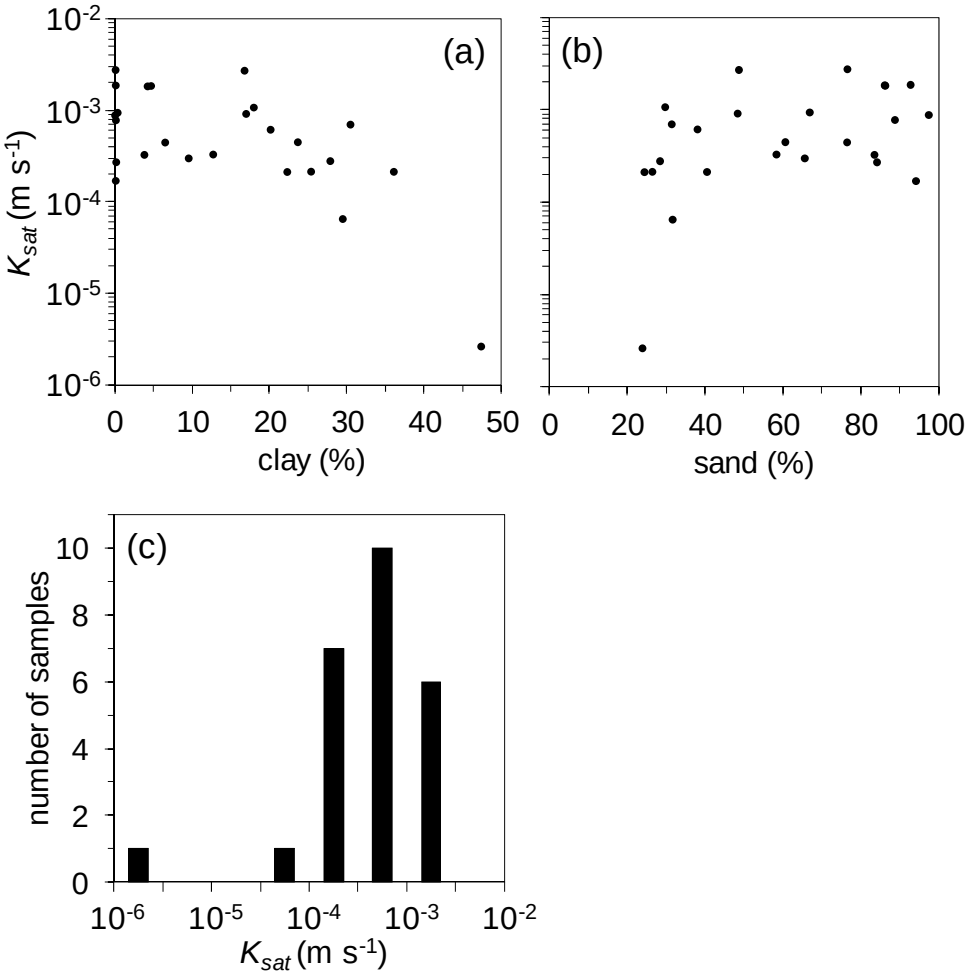

Fig. 18 (a) Relation between Saturated hydraulic conductivity (K_{sat}) and clay fraction of the soil samples from the six sites. (b) Relation between K_{sat} and sand fraction. (c) Frequency distribution of K_{sat}.

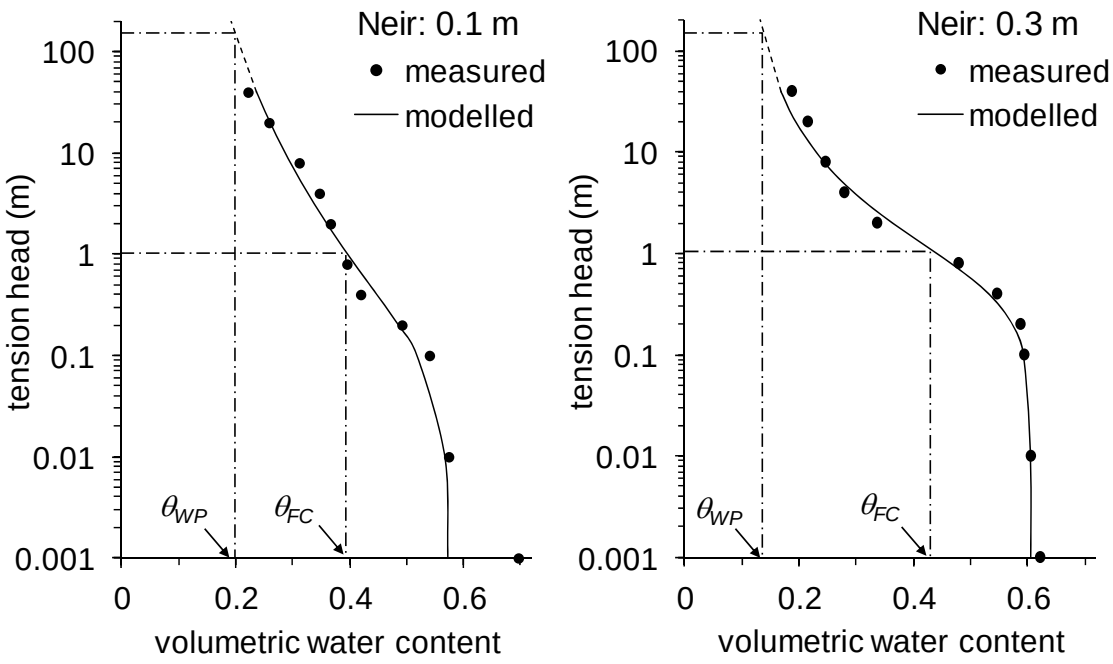

Fig. 19 Examples of water retention characteristic curves for two soil samples from the Neir site. Solid lines indicate the van Genuchten equation with the best-fit parameters. On a preliminary basis, the water content at field capacity (θ_{FC}) is given by the water content at a suction head (= -ψ_m) of 1 m. Similar, the water content at wilting point (θ_{WP}) is given by the water content at a suction head of -150 m.

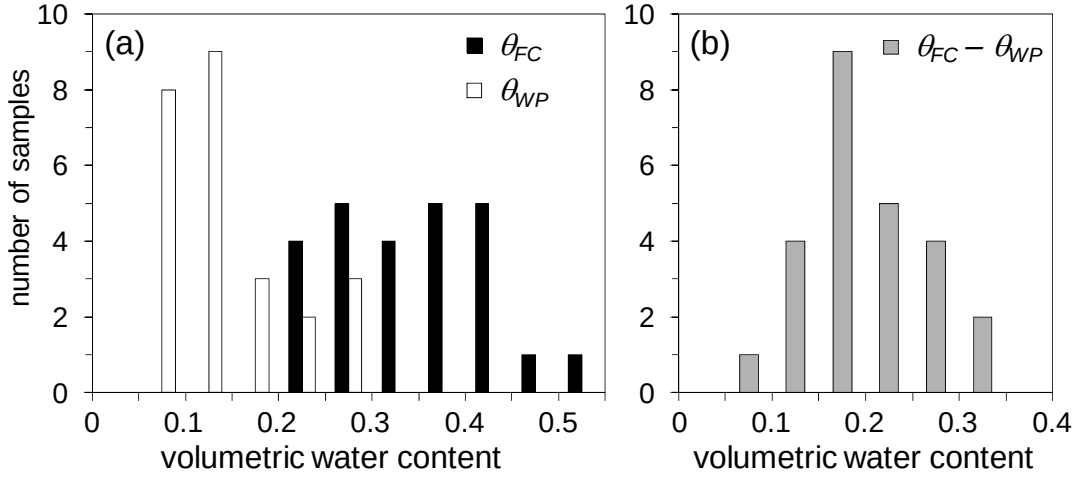

Fig. 20 (a) Frequency distribution of the water content at field capacity (θ_{FC}) and wilting point (q_{WP}). (b) Frequency distribution of the available volumetric water content ($\theta_{FC} - \theta_{WP}$).

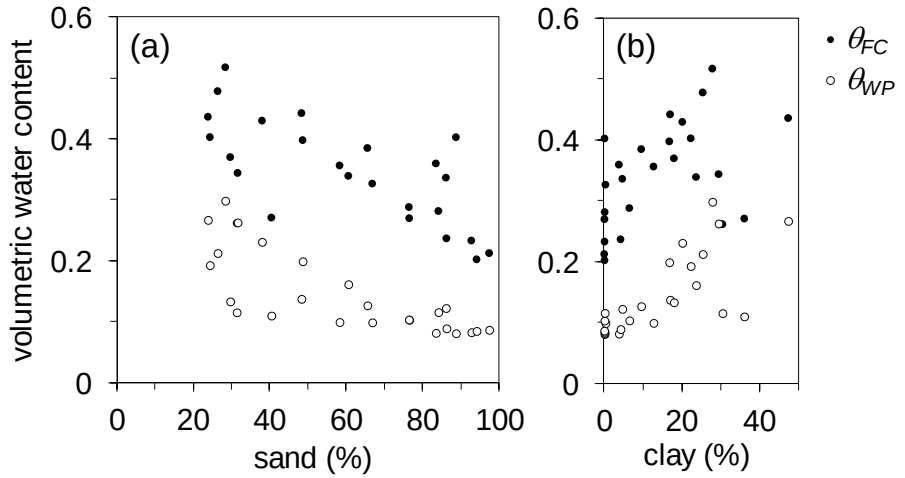

Fig. 21 (a) Relationship between the water contents at field capacity (θ_{FC}) and wilting point (θ_{WP}) and sand fraction. (b) Relationship between θ_{FC} and θ_{WP} and clay fraction.

5 Summary and suggestions

The VSMB simulated evapotranspiration and soil moisture reasonably well when it was tested in the barley field in 2009. The performance of the VSMB was slightly poorer when it was tested in the same barley field in the wet summer of 2011. Its performance could be improved by adjusting the crop root extraction coefficient and the drying curve function, but such adjustment will require extensive data collection and testing. At present, it may be acceptable to use the model with default setting for barley (or spring wheat), as long as the soil water retention parameters and the dates of seeding and harvest are appropriately set to reflect the site condition. It will be useful to test its performance in other locations, where AARD has meteorological and soil moisture data. Such testing will increase the confidence in model simulation results for growing seasons.

The new VSMB model with improved winter process algorithm performed reasonably well when it was tested in the grass pasture site in the three winters of 2006-07, 2007-08, and 2008-09. Future efforts should be made to test the algorithms in other locations, and to incorporate the new algorithms in the VSMB used by AARD for operational purposes.

The analysis of 25 soil samples having a wide range of soil texture indicated significant correlation between soil texture and water retention parameters used in the VSMB. This suggests feasibility of using the pedo-transfer function approach to estimate water retention parameters. However, it is likely that the current number of soil samples may be too small for deriving robust pedo-transfer functions. Future efforts should be made to collect samples from a larger number of locations.

Acknowledgement

We thank Krystal Chin, Joel Steeves, Joe Michielsen, Peter Aukes, Andrew Wiseman, Greg Langston, Nathan Green, Kate Forbes, and John Jackson for field work; Rui Chen and Ligang Xu for earlier model development; Toshihiko Momose for the measurement of soil thermal conductivity; Warren Helgason for providing a tilt-correction program for eddy-covariance data; Ralph Wright and Johanne Boisvert for providing the earlier version of VSMB model and useful suggestions; Jinsheng You for assistance with the UEB model; and Alberta Transportation for the field site access. We also thank Daniel Itenfisu and Larry Bentley for valuable discussion. Funding for the study was provided by Alberta Agriculture and Rural Development, Saskatchewan Watershed Authority, Royal Bank of Canada, Canadian Foundation for Climate and Atmospheric Science (DRI Network), Alberta Environment, Environment Canada Science Horizons Program, and Natural Sciences and Engineering Research Council.

References

Akinremi, O.O., McGinn, S.M. and Barr, A.G., 1996. Simulation of soil moisture and other components of the hydrological cycle using a water budget approach. Canadian Journal of Soil Science, 76: 133-142.

Alberta Agriculture and Rural Development (AARD), 2012. Alberta Soil Information Viewer. http://www2.agric.gov.ab.ca/app77/imf.jsp?site=agrasid (accessed February 13, 2012).

Anderson, P.M., E.A. Oelke, E.A., Simmons, S.R., 1985. Growth and development guide for spring barley. University of Minnesota Agricultural Extension Folder AG-FO-2548. http://www.extension.umn.edu/distribution/cropsystems/DC2548.html (accessed February 14, 2012)

Baier, W., Dyer, J.A. and Sharp, W.R. 1979. The versatile soil moisture budget, Technical Bulletin 87. Agrometeorology Section, Land Resource Research Institute, Research Branch, Agriculture Canada, Ottawa.

Baier, W. and Robertson, G.W., 1966. A new versatile soil moisture budget. Canadian Journal of Plant Science, 46: 299-315.

Bayard, D., Stähli, M. Parriaux, A. and Flühler, H. 2005. The influence of seasonally frozen soil on the snowmelt runoff at two Alpine sites in southern Switzerland. Journal of Hydrology 309: 66-84.

Campbell, G.S. 1974. A simple method for determining unsaturated conductivity from moisture retention data. Soil Science 117: 311-314.

Chen, R., 2008. GIS-based modeling of prairie groundwater recharge in the West Nose Creek watershed. M. GIS project report, University of Calgary.

Dane, J.H. and Hopmans, J.W., 2002. Pressure plate extractor. In: J.H. Dane and G.C. Topp (Editors), Methods of Soil Analysis, Part 4. Physical Methods. Soil Science Society of America Book Series 5, Madison, Wisconsin. pp. 688-690.

de Vries, D.A. 1963. Thermal properties of soil. *In*: van Dijk, W.R. (ed.), Physics of Plant Environment. North Holland Publishing: Amsterdam, pp.210-235.

Environment Canada. 2011. National Climate Data and Information Archive. http://www.climate.weatheroffice.gc.ca/Welcome_e.html [accessed December 21, 2011].

Farouki, O.T. 1981. The thermal properties of soils in cold regions. Cold Regions Science and Technology 5: 67-75.

Flerchinger, G.N. and Saxton, K.E. 1989. Simultaneous heat and water model of a freezing snow-residue-soil system. I. Theory and development. Transaction of the American Society of Agricultural Engineers 32: 565-571.

Gee, G.W. and Or, D., 2002. Laser light scattering (diffraction). In: J.H. Dane and G.C. Topp (Editors), Methods of Soil Analysis, Part 4. Physical Methods. Soil Science Society of America Book Series 5, Madison, Wisconsin. pp. 286-288.

Gray, D.M., Landine, P.G. and Granger, R.J. 1985. Simulating infiltration into frozen prairie soils in streamflow models. Canadian Journal of Earth Science 22: 464-472.

Gray, D.M., Toth, B., Zhao, L., Pomeroy, J.W. and Granger, R.J. 2001. Estimating areal snowmelt infiltration into frozen soils. Hydrological Processes 15: 3095-3111.

Hayashi, M. and van der Kamp, G. 2000. Simple equations to represent the volume-area-depth relations of shallow wetlands in small topographic depressions. Journal of Hydrology 237: 74-85.

Hayashi, M., Jackson, J.F. and Xu, L. 2010. Application of the Versatile Soil Moisture Budget model to estimate evaporation from prairie grassland. Canadian Water Resources Journal 35: 187-208.

Hayashi, M., Goeller, N. Quinton, W.L. and Wright, N. 2007. A simple heat-conduction method for simulating the frost-table depth in hydrological models. Hydrological Processes 21: 2610-2622.

Hillel, D. 2004. Introduction to environmental soil physics. Elsevier Academic Press, San Diego, California, 494 pp.
Hiraiwa, Y. and Kasubuchi, T. 2000. Temperature dependence of thermal conductivity of soil over a wide range of temperature (5-75 °C). European Journal of Soil Science 51: 211-218.
Iwata, Y., Hayashi, M., Suzuki, S., Hirota, T. and Hasegawa, S. 2010. Effects of snowcover on soil freezing, water movement and snowmelt infiltration: A paired plot experiment. Water Resources Research 46, W09504, doi:10.1029/2009/WR008070.
Jackson, J. 2008. A soil water balance and potential recharge study in the north-west Canadian prairies, MSc. thesis, University of Calgary, 136 pp.
Jame, Y.-W. and Norum, D.I. 1980. Heat and mass transfer in a freezing unsaturated porous medium. Water Resources Research 16: 811-819.
Johnson, M.E. and Fitzpatrick, E.A. 1977. Comparison of two methods of estimating a mean diurnal temperature curve during the daylight hours. Arch. Met. Geoph. Biokl. 25: 251-263.
Jordan,. R. 1991. A one-dimensional temperature model for a snow cover: technical documentation for SNTHERM.89. U.S. Army Corps of Engineers, Cold Regions Research and Engineering Laboratory, Special Report 91-16.
Jury, W.A. and Horton, R. 2004. Soil physics, 6th edition. John Wiley & Sons, 370 pp.
Lundin, L.-C. 1990. Hydraulic properties in an operational model of frozen soil. Journal of Hydrology 118: 289-310.
Mayocchi, C.L. and Bristow, K.L. 1995. Soil surface heat flux: some general questions and comments on measurements. Agricultural and Forest Meteorology 75: 43-50.
McKay, G.A. 1964. Relationships between snow survey and climatological measurements. In: Surface Waters, General Assembly of Berkeley, International Union of Geodesy and Geophysics, Publication No. 637: 214-227.
Miller, R.D. 1980. Freezing phenomena in soils. *In* Hillel, D. (ed.) Applications of soil physics. Academic Press, New York, pp. 254-299.
Moore, R.D. 1983. On the use of bulk aerodynamic formulae. Nordic Hydrology 14: 193-296.
Natural Resources Conservation Service (NRCS). 2004. National Engineering Handbook, Part 630 Hydrology, Chapters 4-10, United States Department of Agriculture.
Neitsch, S.L., Arnold, J.G. Kiniry, J.R. and Williams, J.R. 2005. Soil and Water Assessment Tool Theoretical Documentation Version 2005, Grassland, Soil and Water Research Laboratory, Agricultural Research Service, Temple, Texas, 476 pp.
Patron, W.J. and Logan, J.A. 1981. A model for diurnal variation in soil and air temperature. Agricultural Meteorology 23: 205-216.
Priestley, C.H.B. and Taylor, R.J. 1972. On the assessment of surface heat flux and evaporation using large-scale parameters. Monthly Weather Review 100: 81-92.
Puurveen, H., Izaurralde, R.C. Chanasyk, D.S. Williams, J.R. and Grant, R.F. 1996. Evaluation of EPIC's snowmelt and water erosion submodels using data from the Peace River region of Alberta. Canadian Journal of Soil Science 77: 41-50.
Redman, D. 2000. WATTDR user's guide. Waterloo Centre for Groundwater Research, University of Waterloo, Waterloo, Ont. 10 pp.
Reynolds, W.D. and Elrick, D.E., 2002. Falling head soil core (tank) method. In: J.H. Dane and G.C. Topp (Editors), Methods of Soil Analysis, Part 4. Physical Methods. Soil Science Society of America Book Series 5, Madison, Wisconsin. pp. 809-812.
Robertson, G.W., 1968. A biometeorological time scale for a cereal crop involving day and night temperatures and photoperiod. International Journal of Biometeorology, 12: 191-223.

Satterlund, D. R. 1979. An improved equation for estimating long-wave radiation from the atmosphere. Water Resources Research 15:1643-1650.
Schaap, M.G., Leij, F.J., van Genuchten, M.T., 2001. ROSETTA: a computer program for estimating soil hydraulic parameters with hierarchical pedotransfer functions. Journal of Hydrology 251, 163-176.
Schroeder, P.R., Dozier, T.S., Zappi, P.A., McEnroe, B.M., Sjostrom, J.W. and Peyton ,R.L. 1994. The hydrological evaluation of landfill performance (HELP) model, engineering documentation for version 3. EPA/600/R-94/168b, September 1994, U.S. Environmental Protection Agency Office of Research and Development, Washington, DC, 116 pp.
Smith, C.D. 2007. Correcting the wind bias in snowfall measurements made with a Geonore T-200B precipitation gauge and alter wind shield. 87th American Meteorological Society Annual Meeting, San Antonio, Texas, January 13-18, 2007.
Spaans, E.J.A. and Baker, J.M. 1996. The soil freezing characteristic: Its measurement and similarity to the soil moisture characteristic. Soil Science Society of America Journal 60: 13-19.
Stähli, M., Jansson, P.-E. and Lundin, L.-C. 1996. Preferential water flow in a frozen soil- a two-domain model approach. Hydrological Processes 10: 1305-1316.
Stein, J. and Kane, D.L. 1983. Monitoring the unfrozen water content of soil and snow using time domain reflectometry. Water Resources Research 19: 1573-1584.
Tarboton, D.G., Chowdhury, T.G. and Jackson T.H. 1995. A spatially distributed energy balance snowmelt model, Biogeochemistry of seasonally snow-covered catchments. Proceedings of Boulder Symposium, July 1995. International Association of Hydrological Science Publication 228, pp. 141-155.
Twine, T.E. et al. 2000. Correcting eddy-covariance flux underestimates over a grassland. Agricultural and Forest Meteorology 103: 279-300.
van der Kamp, G., Hayashi, M. and Gallén, D. 2003. Comparing the hydrology of grassed and cultivated catchments in the semi-arid Canadian prairies. Hydrological Processes 17: 559-575.
van Dijk, T. 2005. Depression-focused recharge and the impacts of land use on the hydrology of small depressions in Calgary, Alberta, MSc. thesis, University of Calgary, 158 pp.
van Genuchten, M.T. 1980. A closed-form equation for predicting the hydraulic conductivity of unsaturated soils. Soil Science Society of America Journal 44: 892-898.
Watanabe, K. and Wake, T. 2009. Measurement of unfrozen water content and relative permittivity of frozen unsaturated soil using NMR and TDR. Cold Regions Science and Technology 59: 34-41.
Williams, J.R., Duke, P.T., Fuchs, W. Rice O.W. and Taylor, E.D. 1990. EPIC (erosion productivity impact calculator) 2. User's manual. A. N. Sharpley, and J.R. Willims, eds., U.S. Department of Agriculture Technical Bulletin No. 1768, Temple, AZ, 127 pp.
Wilson, K. et al. 2002. Energy balance closure at FLUXNET sites. Agricultural and Forest Meteorology 113: 223-243.
Zaitlin, B., Hayashi, M. and Clapperton, J. 2007. Distribution of northern pocket gopher burrows, earth worms and effects on infiltration in a prairie landscape in Alberta, Canada. Applied Soil Ecology 37: 88-94.